Effect of Mechanical Input Energy on Piezoelectric Energy Harvesting

Master of Science Thesis

Balaji Sankar

TU Delft Delft University of Technology

Effect Of Mechanical Input Energy On Piezoelectric Energy Harvesting

Master of Science Thesis

For obtaining the degree of Master of Science in Materials Science and Engineering at Delft University of Technology

Balaji Sankar

Student Number: 4522435

Decemeber 20, 2018

Delft University of Technology
Faculty of Mechanical, Maritime and Materials Engineering
Department of Materials Science and Engineering

GRADUATION COMMITTEE

Dated: Decemeber 20, 2018

Chair holder:

Dr. Ir. W. Sloof

Committee members:

Prof. dr. P. Groen

Dr. Ir. M.H.F. Sluiter

Abstract

Piezoelectric energy harvesting technology is an alternative source for powering low power electronics. The ability of piezoelectric materials to convert ambient vibrational energy into usable electrical energy is seen as a promising battery-free solution to be used in inhospitable areas to self-power electronics for a longer time with little maintenance.

The goal of this research is to maximise the mechanical input: elastic strain energy experienced by a lead zirconium titanate (PZT) bilayer piezoelectric buzzer by introducing four different boundary conditions during loading. Investigation of how mechanical input from each of these boundary condition influences the stored electrical output is carried out. The effect of three different static loads on each of the stored electrical output for four boundary conditions are studied. In order to accurately compare the data, the mechanical input (elastic strain energy) is calculated while the electrical output (stored energy) is measured experimentally.

Given the brittle nature of ceramics, the maximum load bearing capacity for the PZT ceramic disc is determined by mechanical tests such as the ball-on-the-ring and uniaxial compression tests. This is to ensure that the experiments do not fracture the sample. Results show that, by inducing a bending mode in the buzzer, mechanical input values almost four orders of magnitude higher can be reached when compared to boundary conditions without bending modes. A similar result was found for the stored electrical energy with values for the bending mode of almost three orders of magnitude higher than when no bending is involved.

The comparison between the calculated mechanical input and the measured electrical output shows good agreement in the boundary conditions involving bending. The energy conversion is highly efficient for the full range of applied loads for these boundary conditions. In the case of non-bending boundary conditions, the stored electrical energy is one order of magnitude high than predicted for the mechanical input and thus the model is in poor agreement with experiment.

Keywords: Piezoelectricity, Boundary conditions, Bending of PZT, Electromechanical coupling coefficient (k^2), Ball-on-the-Ring test, Maximum load bearing capacity

Dedicated to:

My Mom and Dad for supporting throughout my life

Contents

List of Figures

List of Tables

Acknowledgement

I would like to take this opportunity to extend my gratitude to the people who have helped me through this research. Firstly, I would thank my supervisor, Prof. dr. Pim Groen from the Department of Aerospace to guide and mentor me through out the entire thesis.

Secondly, I would like to thank my supervisor Dr. Wim Sloof from the Department of 3ME, TU Delft for helping me with the supervision and providing valuable support with the analytical part of the thesis.

I would like to thank Ben Schelen for helping me with the experimental work and providing necessary supporting documents related to the piezometer for conducting experiments.

Also, I would like to thank Dr. Marlies Nijemeisland for supporting with the experiments and measurements.

Special thanks to Jayaprakash for teaching me with the concepts of plate theories.

Thank you Satheesh and sathish for proof reading my report.

Finally, I would like to thank my friends Senthil, Vignesh, Vinod, Shaafi & Deepan and my family in India for supporting me through the hard times.

Nomenclature

U	Mechanical input: elastic strain energy	$[J]$
k^2	Electromechanical coupling coefficient	$[-]$
g	Piezoelectric voltage coefficient	$[Vm/N]$
d	Piezoelectric charge coefficient	$[C/N]$
ϵ_r	Relative permittivity	$[-]$
ϵ_0	Permittivity of free space	$[F/m]$
D	Electrical displacement	$[C/m^2]$
E	Electrical field	$[V/m]$
C	Capacitance	$[F]$
λ	Transmission coefficient	$[-]$
T_c	Curie temperature	$[^\circ C]$
U	Electrical output: stored energy	$[J]$
X	Stress	$[N/m^2]$
s	Compliance	$[m^2/N]$
V_{DC}	Offset voltage	$[V]$
P/F	Load	$[N]$
E	Young's modulus	$[N/m^2]$
ν_i	Poisson's ratio for ith layer	$[-]$
ν	Effective poisson's ratio	$[-]$
t_n	Neutral surface position	$[m]$
F_i	Flexural rigidity of ith layer	$[Nm]$
t_i	Thickness of ith layer	$[m]$
σ_{r_i}	Radial stress for ith layer	$[N/m^2]$
$\sigma_{\theta i}$	Hoop stress for ith layer	$[N/m^2]$
ϵ_{r_i}	Radial strain for ith layer	$[-]$
$\epsilon_{\theta i}$	Hoop strain for ith layer	$[-]$
b	Hertzian contact radius	$[m]$

Chapter 1

Introduction

The Internet of Things (IOT) is an emerging concept in the field of automation used in various domains such as predictive maintenance, transportation systems, health care monitoring and manufacturing systems. The Internet of Things is going to create an ecosystem of connected objects and embedded systems to transfer and share data using sensors. Energy harvesting technologies for power generation are seen as one of the prominent sustainable resources to self power these ultra low-power electronics and wireless sensor networks. Industrial and academic interest on energy harvesting technologies is continuously increasing to replace batteries, especially for structural health monitoring systems used in remote areas which can be inaccessible. The excess time, money and effort required to replace, maintain and service the batteries in these zone can be reduced.

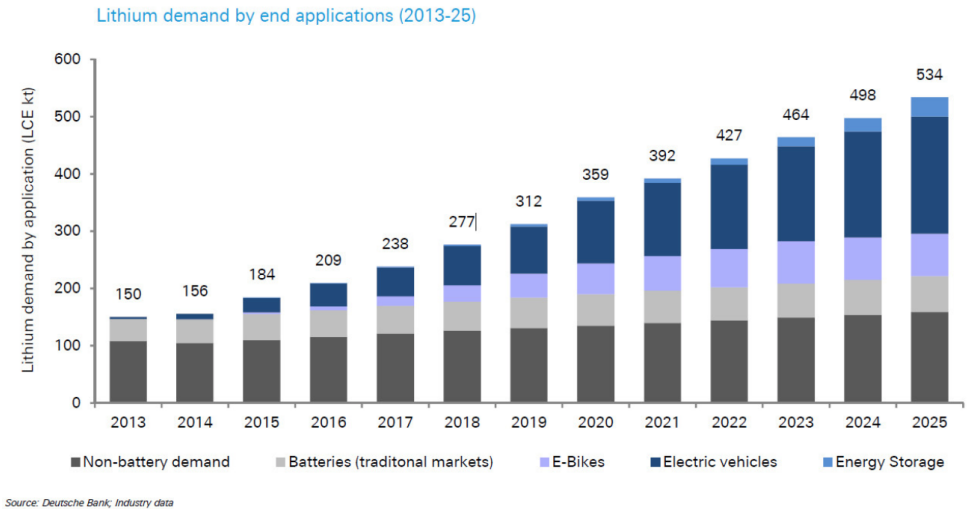

Figure 1.1: Global demand for Lithium
[1]

The production of batteries involves a of lot of energy from the extraction of raw materials to the electricity and fuel consumed during the manufacturing [2]. The demand for lithium, which is the raw material for lithium-ion batteries, is steadily increasing as seen in figure

1.1. It is estimated by the World Economic forum that there will be twice the demand for lithium by the end of 2025 as there is now. The estimated future growth of e-bikes, electric vehicles and energy storage will be using lithium-ion batteries which in turn increases the demand for lithium in the coming years. The current demand for lithium in 2018 is around 277 kilo ton and it will increase to 534 kilo ton in 2025 [1] [2].

The life cycle of lithium, from mining until disposing of batteries involves various environmental hazards such as dust, fumes, waste water, water shortages and toxic spills [2]. The carbon emission associated with the mining of lithium will also increase with the demand in the future. It is essential to replace the use of batteries in certain applications with more sustainable power sources.

Battery-less solutions can be provided by energy harvesting devices. The process of energy harvesting includes extracting energy from naturally available energy sources and converting them in to a useful form of energy to further store and utilise them. Various forms of energy that can be scavenged are thermal, mechanical, solar, wind, wave and acoustic. One prominent method is to use piezoelectric materials for the purpose of energy harvesting [3] [4] [5] [6]. The unused vibrational energy from the environment to be converted into useful electrical energy [2].

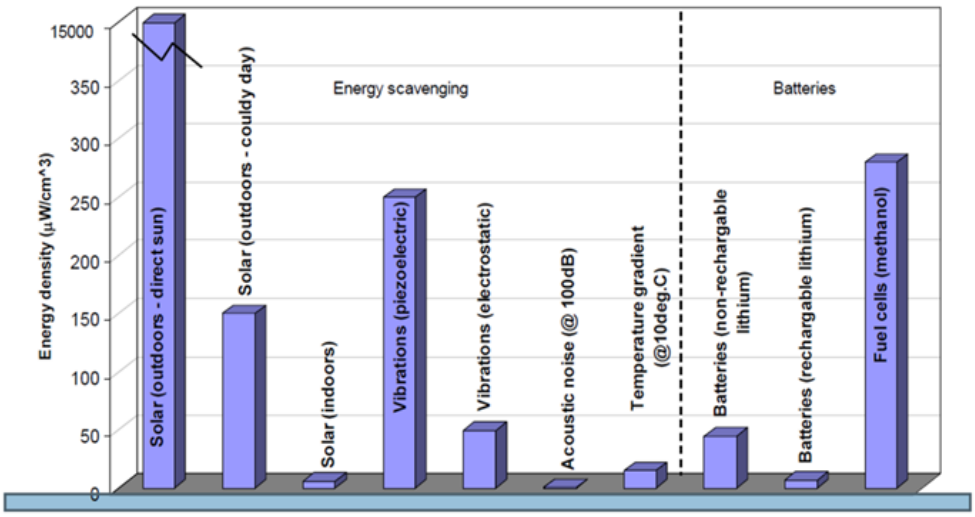

Figure 1.2: Power density comparison for various energy scavenging techniques [7]

The power density of various energy scavenging techniques is compared in the figure 1.2. From this comparison, it can be seen that piezoelectric energy scavenging of ambient vibrations is second only to solar in the available energy density. Since direct exposure to sunlight is not always possible, it shows that the power density for the vibrational piezoelectric will be able to power devices better when operated indoors, low lighting and in vibrational environments. Piezoelectric energy harvesting technique can be a best

alternative to batteries due to its high power density. Piezoelectric energy harvesting is also attractive in situations where unused power is available in the absence of sunlight. Vibration from human motion, machinery vibration, structural vibration, etc are used for the piezoelectric energy harvesting.

Employing piezoelectric energy harvesting techniques instead of batteries would be a suitable choice for powering ultra-low power electronics and other wireless sensors because they are small when compared to other energy harvesting technologies. Also, the minimal energy scavenged from a small size piezoelectric buzzer would be sufficient to power these devices. [8]

The piezoelectric energy harvesting method comprises of three main steps:

- Kinetic energy of the mechanical load to mechanical input energy conversion
- Mechanical energy to stored electrical energy transduction
- Stored electrical energy to electrical output energy transfer [9], [10], [11], [12], [13], [14], [15].

In the first step, the non-translation energy in the piezoelectric material is produced by converting the inertial or kinematic energy of the external source applied on the piezoelectric material. Choosing the right mechanical design for the piezoelectric material will help in maximising the strain. Proper mechanical impedance matching is one of the important factors to be considered [16].

The electromechanical coupling coefficient (k^2), which is the ratio between stored electrical energy and input mechanical energy or vice versa, governs the transduction between the mechanical and electrical energy in the piezoelectric material. Lead zirconium titanate (PZT) is a widely used piezoelectric ceramic with k^2 of about 0.5 [17]. The figure of merit of the piezoelectric harvesters is not based on the k^2, as commonly accepted for the vibrational harvesters however but on $d{\cdot}g$, where d is the piezoelectric charge coefficient and g is the piezoelectric voltage coefficient [16].

In the third step, the stored electrical energy in the piezoelectric material is harvested as electrical output energy. The transfer of the stored energy to the outside world is done by using an electrical circuit consisting of rectifying diodes or inductive coils. The stored output energy can be influenced by altering the boundary conditions of the applied mechanical load [17].

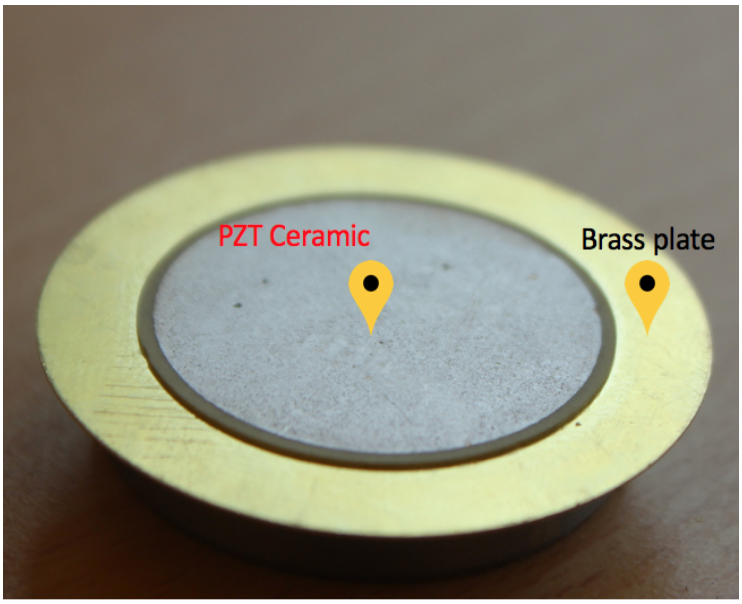

Figure 1.3: PZT piezo buzzer used for experiments

The piezoelectric material used in this study is lead zirconium titanate (PZT) ceramic, which is brittle in nature. The PZT ceramic is glued to a brass plate. Bending can be induced now in the structure to optimise strain and harvest the maximum output electrical energy. This bilayer piezoelectric is shown in the figure 1.3. The dimensions of the buzzer and the material properties will be discussed in the chapter-4.

1.1 Objective and scope of the thesis

It is evident from the literature that the electromechanical coupling coefficient (k^2) value for a PZT ceramics is about 0.5, which is a high value when compared to the value of other piezoelectric materials and composites [18, 19]. To utilise the advantage of high k^2 value and imposing a higher strain on the PZT ceramic buzzer is quite challenging because the PZT ceramics are brittle in nature, which limits them to be loaded in tensile condition. But PZT ceramics can withstand higher load in compression. The compressive strength of the PZT ceramics is >517 MPa in real environment, it is higher than the tensile strength of 74.8 MPa [20]. The main scope of this thesis is considering these limitations and the study is carried out for maximising the strain to harvest maximum stored electrical energy in the PZT ceramics for four different boundary conditions. Determination of mechanical failure load for the PZT ceramic buzzer in these four different boundary conditions are also studied.

The main research questions are

1. To investigate the electrical output: stored energy for the PZT ceramics experimentally by applying the quasi-static load with the piezometer system in the four different boundary conditions and to study how these boundary conditions influences the stored electrical energy.

2. To investigate the mechanical input: elastic energy analytically for PZT ceramics subjected to four different boundary conditions.

3. To study the comparison between the mechanical input: elastic strain energy to electrical output: stored energy for the PZT ceramics in the four different boundary conditions.

4. Finally, to investigate how the maximum load bearing capacity for PZT ceramics varies in four different boundary conditions by conducting mechanical tests such as ball-on-the-ring and uniaxial compression test.

1.2 Chapter overview

This introductory chapter describes why piezoelectric energy harvesting is an attractive alternative for batteries and other energy scavenging methods. The three main steps involved in the piezoelectric energy harvesting are provided. Finally the objective and research questions of this thesis is portrayed.

The second chapter introduces the background study on piezoelectricity and on lead zirconium titanate (PZT) material and its properties. An overview of the other essential piezoelectric coefficients are also presented.

In the third chapter, detailed information on the piezometer setup and its working principle are presented in the first part. The mechanical testing setup and its working procedure are dealt in the second part of this chapter.

The fourth chapter is divided in to four subsections. The first part discusses the result of experimentally measured electrical output: stored energy for PZT ceramics in four different boundary conditions. The second part is focused on the maximum mechanical load bearing capacity of the PZT in four different boundary conditions. The third part discusses the results of the analytically calculated mechanical input: elastic energy for the four different boundary conditions. The fourth part discuss the conversion between the mechanical input energy and the electrical stored energy for all the boundary conditions.

The fifth chapter concludes the answers for all the research questions mentioned. Recommendations for future work are presented.

Chapter 2

Background study on the piezoelectric materials

2.1 Piezoelectricity

Materials with non-centrosymmetric crystal structure can exhibit the piezoelectric effect. It is observed only in the dielectric materials. The piezoelectric effect was first discovered in the year 1880 by the French physicist Pierre Curie, working with his brother Jacques. When a mechanical load is applied on this non-centrosymmetric material, electric charges are generated on the surface of the material and vice versa. In other words, the ability of the material to convert mechanical energy into electric energy and vice versa is known as piezoelectric effect [17], [21], [22] [23]

The piezoelectric behaviour can be classified into the direct piezoelectric effect and the inverse piezoelectric effect.

2.1.1 Direct piezoelectric effect

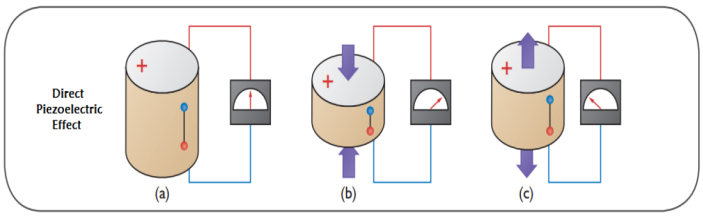

Figure 2.1: Direct Piezoelectric effect
[22]

When a mechanical or compressive load is applied on the piezoelectric material, the center of positive and negative charge shift with respect to each other at the microscopic level and an electric charge is generated on the surface of the material. This effect is known as

the direct piezoelectric effect [21], [23], [24] and it is shown in the figure 2.1. The linear constitutive equation for direct piezoelectric effect is as follows [17, 21, 25]:

$$D = dT + \epsilon^T E \tag{2.1}$$

where,

T : applied stress

d : piezoelectric charge constant

E : applied electric field

D : electric displacement

ϵ^T : relative permitivitty or dielectric constant of the material under constant stress

2.1.2 Inverse piezoelectric effect

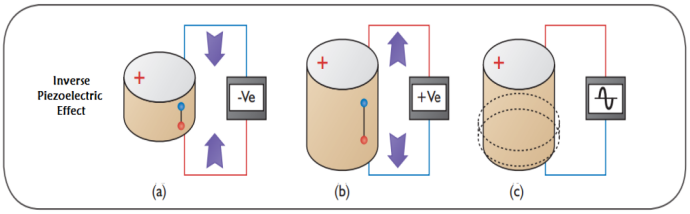

Figure 2.2: Inverse piezoelectric effect
[22]

The inverse piezoelectric effect is shown in the figure 2.2, which is the opposite of the direct piezoelectric effect. When an electric field is applied on the piezoelectric material, an electrical displacement of the ion happens at the microscopic level and it gets geometrical deformation in the macroscopic level [23], [24]. The constitutive equation for indirect effect is as follows [17, 21]:

$$S = s^E T + dE \tag{2.2}$$

where,

S : the strain i.e. relative deformation

s^E : compliance, inverse of elasticity, under constant electric field E.

2.2 Piezoelectric coefficients

Various piezoelectric coefficients and their physical meaning that are useful for this thesis will be discussed in this section.

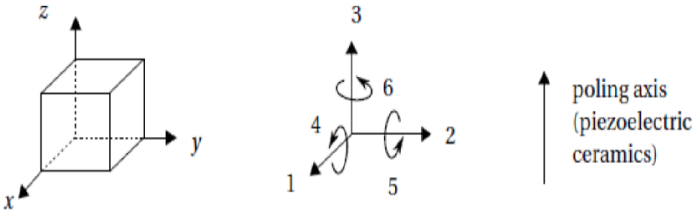

Figure 2.3: Designation of the axes and direction of deformation [21]

The axis nomenclature used to describe the piezoelectric coefficients is shown in the figure 2.3. The subscripts used in describing the piezoelectric coefficients will be i and j. The subscript i denotes the direction of the electric quantity (either the electric displacement or the electric field). The subscript j denotes the direction of the mechanical quantity (either the strain or the stress).

2.2.1 Dielectric coefficient (ϵ_{ij})

The charge per unit area in the j-axis due to the applied electric field in the i-axis is determined by the Dielectric coefficient (ϵ_{ij}) [22]. The relative dielectric constant (ϵ_r) is proportional to the capacitance C, and the thickness d. It is inversely proportional to the electrode area A.

$$C = \frac{\epsilon_r.\epsilon_o.A}{d} \tag{2.3}$$

where ϵ_o is the permittivity of free space = 8.854×10^{-12} F/m

2.2.2 Piezoelectric charge coefficient (d_{ij})

The piezoelectric charge coefficient (d_{ij}) is defined as the polarization generated due to the electric displacement (D_i) the material for the applied mechanical stress (T_j), under zero electric field. This is direct piezoelectric effect.

$$D_i = d_{ij} \times T_j \tag{2.4}$$

d_{31} configuration is used for loading the piezoelectric buzzer in bending for this thesis [21] , [8], [22].

2.2.3 Piezoelectric voltage coefficient

The piezoelectric voltage constant (g_{ij}) is the electric field (E_i) generated in the i-direction per unit of mechanical stress applied (T_j) in the j-direction [8]. In energy harvesting appliations, piezoelectric voltage coeeficient is an important parameter [22], [8].

$$E_i = -g_{ij} \times T_j \tag{2.5}$$

The piezoelectric charge constant and the voltage constant are related to each other according to:

$$g_{ij} = \frac{d_{ij}}{\epsilon} = \frac{d_{ij}}{\epsilon_r \epsilon_o} \tag{2.6}$$

where, ϵ_0 is the permittivity in vacuum and ϵ_r is the relative permittivity. Both these constants are temperature dependent [8].

2.2.4 Piezoelectric coupling coefficient

Other coefficient for the piezoelectric material is the piezoelectric coupling coefficient (k^2). It governs the transduction between the mechanical and electrical energy in the piezoelectric material. It is a ratio between stored mechanical energy and input electrical energy or vice versa [17].

$$k^2 = \frac{\text{Mechanical energy converted into stored electrical energy}}{\text{Input mechanical energy}} \tag{2.7}$$

2.2.5 Transmission coefficient, (λ)

As we know, the piezoelectric capacitor can convert the mechanical energy into electric energy and vice versa. The transmission coefficient, λ, is the ratio of output electrical energy over input mechanical energy and vice versa [17].

$$\lambda = \frac{\text{Output electrical energy}}{\text{Input mechanical energy}} \tag{2.8}$$

2.2.6 Figure of Merit of a piezoelectric energy harvester

The Figure of Merit of a piezoelectric energy harvester is explained as follows. When a mechanical load is applied on the piezoelectric transducer, the stress due to the load induces strain in the material. This applied load generates a mechanical input energy of $1/2\text{sX}^2$ [17], where s is the compliance and X is the force applied. This elastic strain energy is used to charge the piezoelectric capacitor. This leads to a stored electrical energy of

$$U_{open} = \frac{1}{2} \times dgX^2 \tag{2.9}$$

The transmission coefficient is the ratio between the output electrical energy to input mechanical energy. The piezoelectric energy harvester is optimised to obtain the the maximum transmission coefficient to harvest the stored mechanical energy. A fraction of $k^2/(4\text{-}2k^2)$ of the absorbed mechanical energy can be harvested. The maximum transmission coefficient is given as follow: [17]

$$\lambda_{max} = \left[\frac{1}{k} + \sqrt{((1/k)^2 - 1))}\right]^{-2} \approx k^2/\left(4 - 2k^2\right) \tag{2.10}$$

The derivation of the maximum transmission coefficient is out of scope for this thesis and it is shown in the literature [17].

The maximum output energy is given as:

$$U_{out,max} = \frac{1}{2}sX^2 \cdot \frac{k^2}{(4 - 2k^2)} = \frac{k^2}{(4 - 2k^2)} \cdot \frac{1}{2}dgX^2 = \frac{1}{(4 - 2k^2)}U_{open} \tag{2.11}$$

It is a fraction of $\frac{1}{(4-2k^2)}$ of the stored elecrical energy in open circuit. Depending on k^2 the fraction varies between 1/2 to 1/4. Therefore the figure of merit of the piezoelectric energy harvester is equal to d.g and does not depend on the compliance of the material.

2.3 The origin of piezoelectricity and perovskite single crystal structure of PZT

Lead zirconium titanate, PZT, crystallises in perovskite crystal structure and can be described by the chemical formula ABO_3 [17], [23], [26]. The perovskite crystal structure consists of A and B cations which are of different size. The A cations have a larger atomic radius than the B cations. The A cations occupies the corners of the unit cell and the B cations occupies the center of the unit cell. They are positively charged ions. In the case of PZT, Pb^{2+} and Ti^{4+}; Zr^{4+} are the cations. The O^{2-}anion, which is a negatively charged ion occupies the face center of the unit cell.

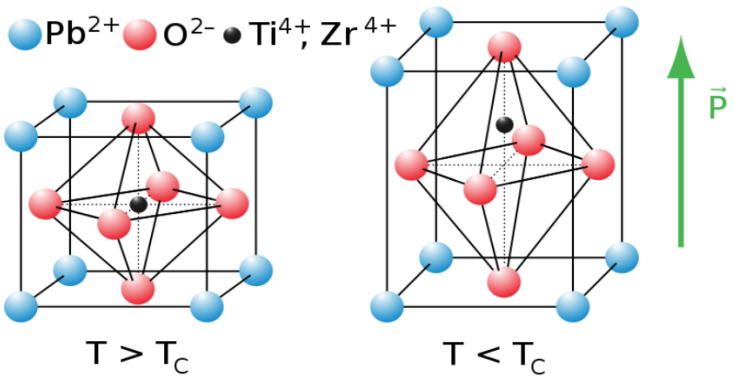

Figure 2.4: PZT perovskite crystal structure
[27]

Figure 2.4 shows the perovskite crystal structure. The phase of the perovskite crystal depends on the temperature. Below the Curie temperature T_c, the Zr^{4+},Ti^{4+} cation is not at in the centre of the six oxygen anions at the face centre of the unit cell. This gives rise to to the permanent electric dipole by forming a tetragonal unit cell [28]. Above the Curie temperature T_c, the unit cell changes from tetragonal to cubic because the Zr^{4+},Ti^{4+} cation is in the centre of the six oxygen anions. [22]. Above the Curie temperature the piezoelectric material loses its piezoelectric properties [17].

2.4 Piezoelectric ceramics

The most widely used piezoelectric ceramic is Lead Zirconate Titanate (PZT) due to its excellent piezoelectric properties. These PZT ceramics exhibits ferroelectric properties.

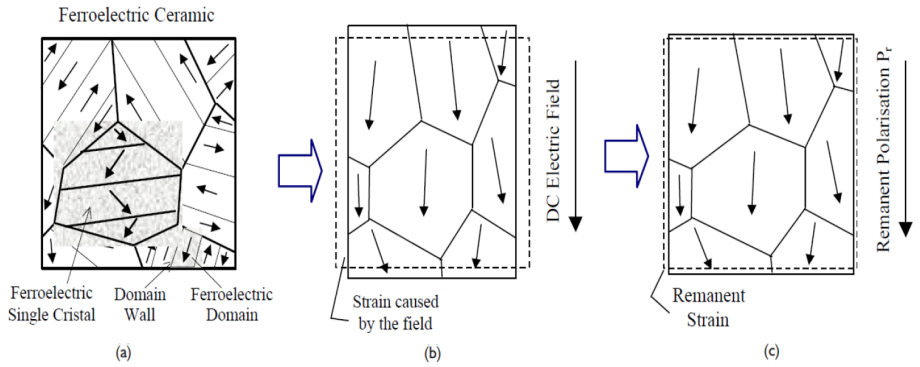

Figure 2.5: Schematic illustration of the Poling process
[22]

The collection of single crystals can be considered as ferroelectric grains, which has a random orientation of ferroelectric domains and do not posses any piezoelectric properties

and net polarization before poling. The schematic illustration of the ferroelectric ceramics before poling is shown in the figure 2.5 (a). The domains are seperated by a boundary called domain walls. The boundaries between the domain are known as 90°or 180°domain walls [26].

The ferroelectric ceramic is subjected to a poling treatment in order to align the ferroelectric domain/ dipoles in the required direction by applying a strong external electric field. Very few domains are not perfectly aligned to the application of electric field due to the presence of intergranular stresses. This results in aligning partially or do not align by keeping the polarity of the domains in their initial positions. The other reason for preventing the reorientation of these dipole would be crystal imperfection causing a strain within the grain [22]. Figure 2.5(b) illustrates the strain caused in the polycrystalline ceramic by applying an electric field. Remanent polarisation and remanent strain are maintained in the ferroelectric ceramic after removing the external electric field [21], [26] .

The ferroelectric ceramic after the poling process is shown in figure 2.5(c). Now the polycrystalline ceramic exhibits piezoelectric behaviour and its maintained as long as the material is not subjected above the Curie temperature. If it is subjected above the Curie temperature of 350°C, the cubic crystal structure transforms into centrosymmetric and results in losing the piezoelectric properties [21].

The chemical modification by doping can enhance the properties of the PZT ceramics. This chemical modification further classify the material into soft and hard ceramics based on the type of dopants added [24]. Easy poling process, better dielectric and piezoelectric properties are obtained in the soft PZT ceramics due to the presence of cationic vacancies. This makes the domain wall move easily and further lowers the coercive field. These cationic vacancies are formed as a result of replacing few of the $A^{2+}$and B^{4+} sites in the perovskite crystal structure with higher valent cations [24]. This is called as donor doping.

Acceptor doping results in achieving the hard PZT ceramics, where few of the B^{4+}cations are replaced with lower valent cations. Anionic oxygen vacancies are formed in the crystal structure. These anionic vacancies pin the domain wall to the oxygen vacancies and make the PZT ceramics difficult to pole and further lower the piezoelectric properties but also lower the dielectric losses [24]. Due to the superior piezoelectric properties and easy poling process, soft PZT ceramics are used in the sensing and energy harvesting applications. Hard PZT ceramics are used in applications that requires a high Curie temperature [24].

2.5 Background study on optimising the strain in the mechanical design

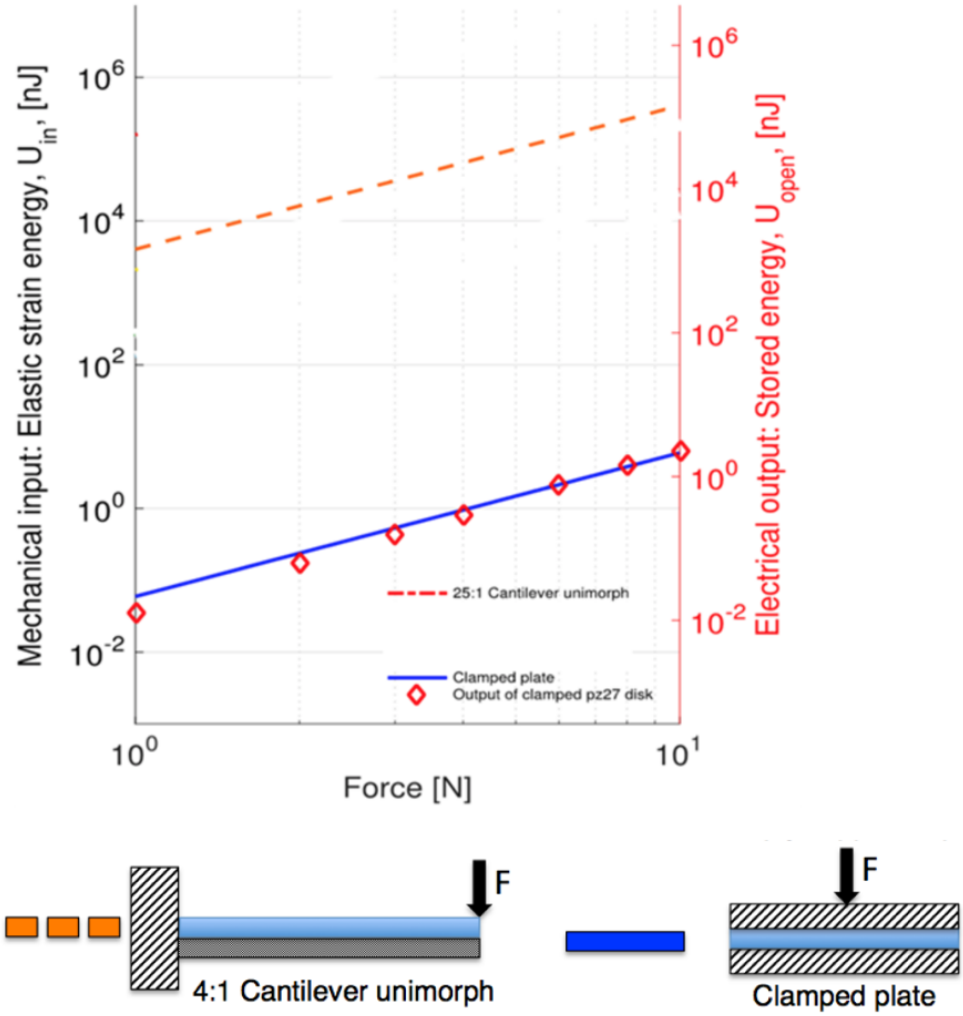

Figure 2.6: Comparison of Mechanical input: Elastic strain energy,U (J) and Electrical output: Stored energy,U (J) for PZ27 in different boundary conditions
[17]

Several studies are being carried out to enhance the mechanical design for maximising the strain and on maximising the electromechanical coupling coefficient, k^2, of the piezo transducer [29–34]. The study carried out by Deutz [17] compares the mechanical input: elastic strain energy, electrical output: stored energy and its transduction for various boundary conditions. PZ27 ceramics were used as a sample in the study. The open

diamond markers in figure 2.5 represent the mechanical input and electrical output values for the clamped PZ27 disk. One of the important conclusion from [17] was that the stored electrical energy per unit volume for the clamped PZ27 disc is independent of the thickness used. This conclusion was obtained from testing a PZ27 ceramic discs with the thickness of 0.5 mm and 1 mm for the diameter of 10 mm and 20 mm.

Next, the clamped rectangular plate was used for testing the mechanical input: elastic strain energy. The mechanical input and electrical output: stored energy results obtained for this condition is almost same as the results obtained for the clamped disc condition. The results for clamped rectangular plate is indicated with the blue line in figure 2.5. The result obtained for this condition is in good agreement with the $1/2\times\ d_{33}g_{33}(F/A)^2$.

The study by Deutz was further extended to test a unimorph cantilever PZ27 plate, which consists of one active layer and one inactive layer. The unimorph cantilever condition was chosen to induce bending in the plate. The aluminium (Al) plate of equal width and length was bonded to the PZ27 ceramic plate to prepare a cantilever unimorph. The aluminium (Al) plate is an inactive substrate and it is used to enhance the bending. The thickness of the aluminium plate was chosen in such a way that the neutral axis of the unimorph coincides with the interface between the piezoelectric plate and aluminium substrate [17]. The unimorph cantilever plate condition induces about 4.5 order of magnitude higher input elastic strain energy and stored electrical energy when compared to clamped disc and clamped rectangular plate boundary conditions.

From the knowledge obtained from [17], we extended our study in this thesis by using a PZT piezoelectric ceramic disc loaded in four different boundary conditions. These four different boundary conditions are explained in detail in chapter-3. The respective analytically calculated input strain energy and measured stored electrical energy are discussed in chapter-4.

Chapter 3

Experimental set-up & procedure

The main focus of this chapter is to describe the experimental procedures and the working principles behind the piezometer system used for measuring the electrical output: stored energy,U (J) in the piezoelectric buzzer tested for four different boundary conditions with three different pre-static loads of 10 N, 11.4 N and 13.4 N.

The second part of this chapter describes the four different mechanical boundary conditions for loading the piezoelectric buzzer used in this work.

Finally, the working principles of the mechanical test conducted such as ball-on-the-ring test and compression test are discussed in the third part of this chapter.

3.1 Experimental setup and working principle of the piezometer system

The piezometer system is a customised setup to measure the electrical output: stored energy in any piezoelectric material more accurately and sensitively in the order of nJ/cm^3. The schematic of the piezometer system operating in a quasi-static load is shown in figure 3.1 and 3.2.

The piezoelectric buzzer is loaded in four different boundary conditions and it is placed in between the two spherical metal calibers PM300 placed identical to each other. Both static and dynamic force ($F(\omega t)$=$F_{max}f(\omega t)$, where $f(\omega t)$ is a periodic function, t is the time and ω the angular frequency) are supplied from the Agilent 33210A function generator. The piezoelectric charges are generated on the surfaces of the piezoelectric sample ($Q(\omega t)$=$Q_{max}f(\omega t)$ due to the application of the dynamic force.

With this piezoelectric system, the short circuit current, $I_{SC}(\omega t)$ and open circuit voltage, $V_{OC}(\omega t)$ can be measured. In our case, open circuit voltage $V_{OC}(\omega t)$ is measured with bypassing the measurement select switch (bubble 4, fig 3,2). Therefore the guarded cables are used to transfer the charges, $Q(\omega t)$ to Keithely 6517b electrometer.

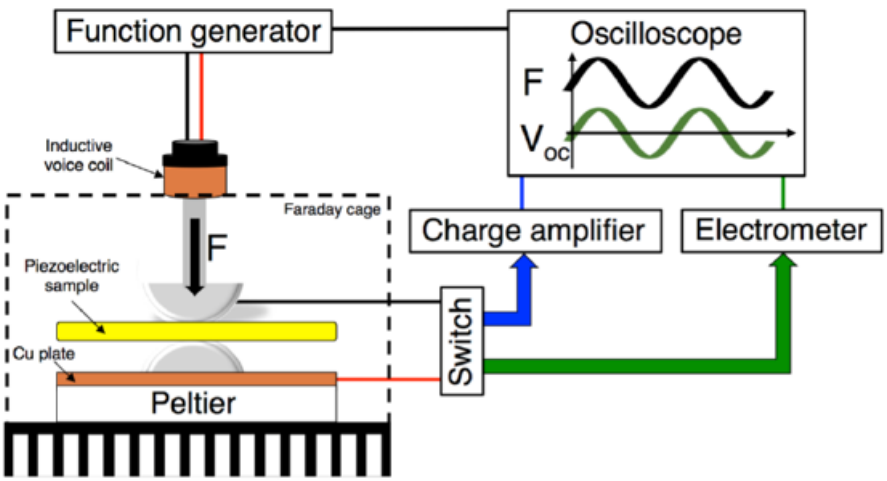

Figure 3.1: Schematic representation of the piezometer system [17]

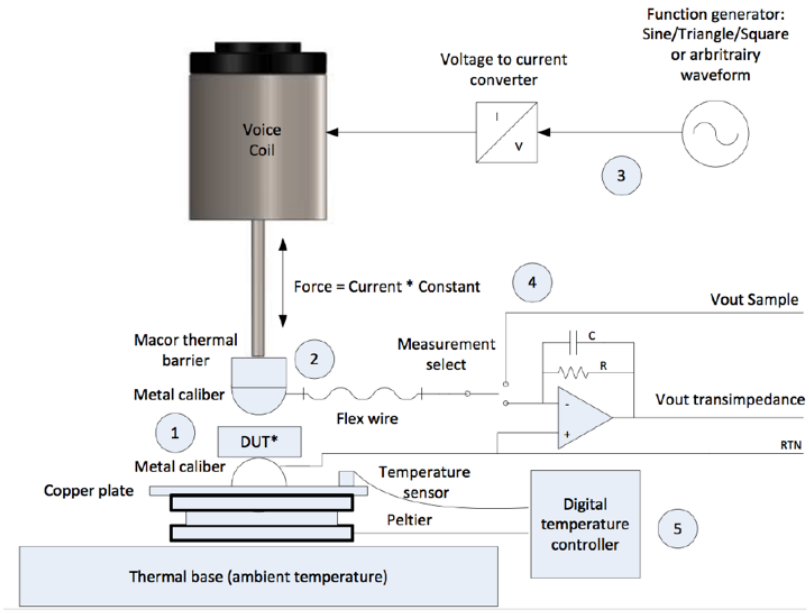

Figure 3.2: Schematic representation of piezometer with a simplified peripheral electronics [17]

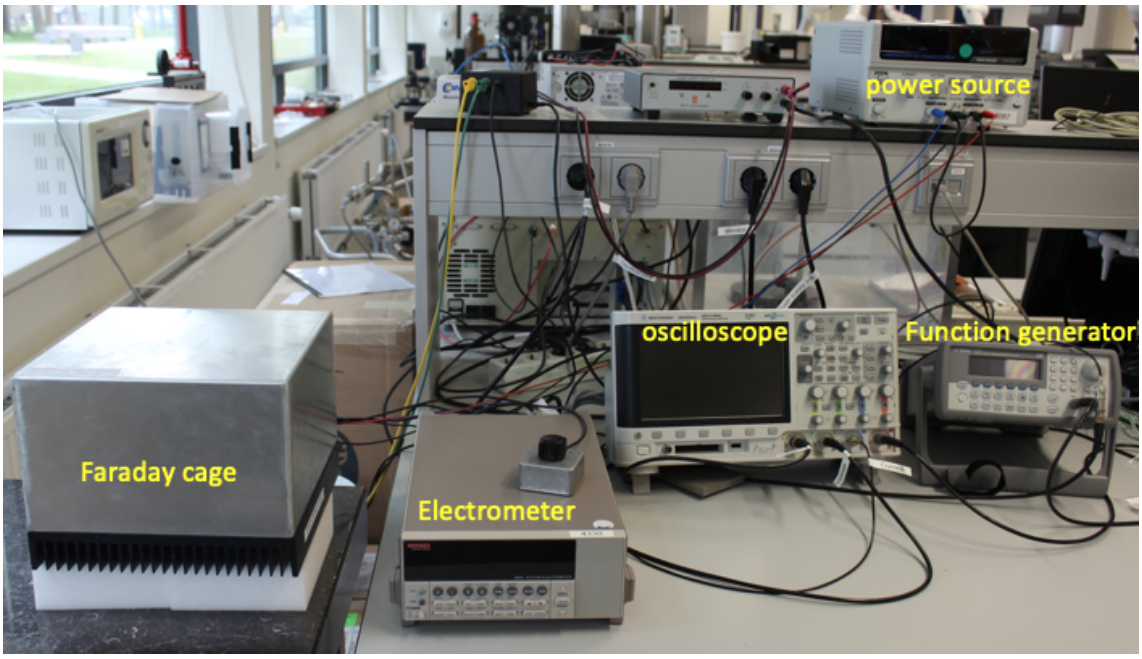

Figure 3.3: Piezometer system

The piezometer system consist of Faraday cage , Agilent 33210A function generator, Keithley electrometer (Cleveland, Ohio, USA), and a digital storage oscilloscope (DSO-X-2004A). The various components of the piezoemeter system are explained in detailed in the further subsections.

3.1.1 Faraday cage

The Faraday cage consists of inductive voice coil, Berlincourt calibers, copper plate and Peltier element as shown in figure 3.1. The inductive voice coil, which is placed inside the Faraday cage converts the input electrical signal from the function generator Agilent (33210A) into a quasi static mechanical force. This quasi static mechanical force is further used to drive the metal rod connected to the voice coil. The force from the metal rod is applied to the piezoelectric buzzer using a spherical metal caliber. The thermal and electrical isolation from the sample to the metal rod is provided by the Macor mount, which is placed in between the metal rod and a metal caliber. The piezoelectric buzzer is loaded in four different boundary conditions and it is placed in between the two spherical metal calibers PM300 placed identical to each other. No:2 in the figure 3.2 and the figure 3.4 indicates the piezoelectric buzzer located between the metal calibers and the metal caliber that is connected to the metal rod from the voice coil can be seen.

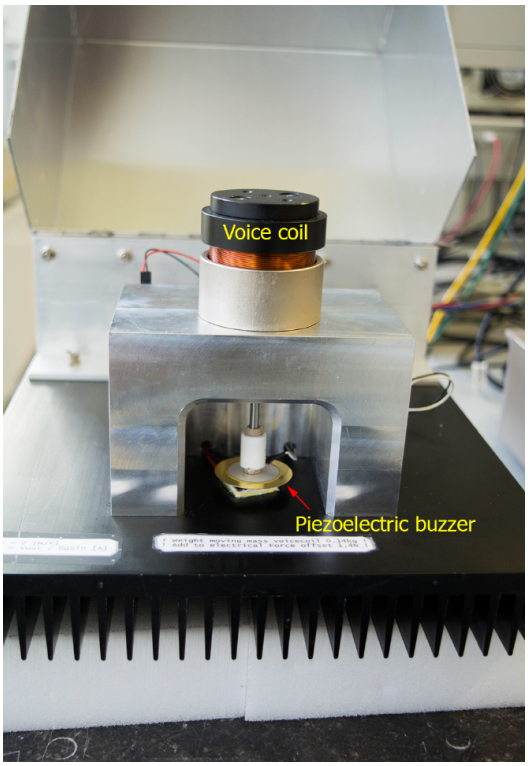

Figure 3.4: Picture of the piezotester [8]

Another Berlincourt metal caliber is connected to the copper plate and the Peltier heating & cooling element is placed below the copper plate. A temperature sensor is connected to the copper plate. During the high frequency application of the mechanical force, the metal caliber is heated and the copper plate serves the purpose of distributing the temperature uniformly. The Peltier actuated temperature controller is used to regulate the temperature of the caliber by comparing it with the setpoint temperature and to further heat or cool the metal caliber.

3.1.2 Agilent 33210A function generator

The electrical signal required to drive the voice coil is given from the Agilent 33210A function generator. The change in the mechanical input: elastic strain energy and the electrical output: stored energy of the piezo buzzer loaded in four different boundary conditions loaded in the low frequency range of 1 Hz to 10 Hz is the prime focus of this thesis. Therefore for each specific frequency from 1 Hz to 10 Hz (in the interval of 1 Hz), the amplitude of the sinusoidal wave is varied from 0.5 V to 10 V with an increment of 0.5 V is provided as an input for each boundary condition.

Increasing the amplitude of any given frequency results in increasing the energy of the input sinusoidal wave frequency.

In order to convert the amplitude in terms of quasi static force (N), the relationship is given by:

$$\text{Quasi static Force applied (N)} = 2\times\text{Amplitude} \tag{3.1}$$

Therefore, increasing the amplitude of the input sinusoidal wave for any given frequency increases the quasi static force applied on the piezo buzzer. The voice coil exerts a pre-static load of 1.4 N during the application of the quasi-static force because of its own weight.

The experiment for each boundary condition is carried out with 3 different offset voltage (4.3 V, 5 V and 6 V). Thus the change in DC offset voltage(V_{DC}) contributes to the change in the pre static load applied. The DC offset voltage is converted in terms of the static load (N) by the relation

$$\text{Static Load (N)} = (2 \times V_{DC}) + 1.4 \text{ N} \tag{3.2}$$

If the offset DC voltage value is set to 0, then there would be only 1.4 N pre-static load to the piezo buzzer. If the offset is set to 4.3 V, the pre static load applied would be 10N and for 5 V and 6 V, the pre static load applied would be 11.4 N and 13.4 N respectively.

Therefore, if we say one newton force is applied to the piezobuzzer structure in any boundary condition that would be equal to the summation of static pre-load due to the DC offset voltage , static load exerted by the voice coil and the input quasi static force of one newton applied for that particular frequency .

$$\begin{aligned}\text{Force applied (N)} =&\text{Static load due to offset voltage} + \text{ Static load exerted by voice coil}\\ &+ \text{Quasi static force applied}\end{aligned}$$

3.1.3 Keithley electrometer and digital storage oscilloscope

The metal calibers in the faraday cage are connected to the Keithley electrometer (Cleveland, Ohio, USA). This electrometer is used to measure even extremely low voltages generated due to the direct piezoelectric effect on the piezoelectric buzzer for different boundary conditions. Also, the guard function in the electrometer is turned on to minimise the leakage errors while measuring.

The electrical signal from the function generator is given to perform the mechanical work on the piezoelectric buzzer. The generated open circuit voltage by the piezoelectric buzzer, V_{OC}, is measured by the electrometer and further displayed in the form of sinusoidal wave in the DSOX2002A oscilloscope.

The generated open circuit voltage in the piezo buzzer , V_{OC}, is measured for the increasing amplitude range from 0.5 V to 10 V with the increment of 0.5 V for all the low frequency range between 1 Hz to 10 Hz. This measurement is repeated for all four boundary conditions subjected to three different DC offset voltage.

These measured output open circuit voltage , V_{OC}, are further used to calculate the electrical output: stored energy in the PZT capacitor for all four boundary conditions subjected to three different static loadings.

$$\text{Electrical Output: Stored Energy, U(J)} = \frac{1}{2} \times C \times V^2 \tag{3.3}$$

The calculated electrical output: stored energy for a particular amplitude in all the frequency values between 1 to 10 Hz is averaged out to find the average electrical output: stored energy.

3.2 Mechanical boundary condition of the piezoelectric buzzer

The four different mechanical boundary conditions of the piezoelectric buzzer loaded between the Berlincourt metal calibers are discussed in this section. The change in the mechanical input: elastic strain energy and the electrical output: stored energy of the piezoelectric buzzer when loaded in four different mechanical boundary conditions for the force applied are studied.

3.2.1 Boundary condition-1

In the boundary condition-1, the piezo buzzer is placed on the rigid flat surface with no support. The PZT layer is on the top position to make a concentrated contact with the metal caliber of the piezometer and the brass is in the bottom position resting on the rigid flat surface. The bending of the piezo buzzer structure is not possible in this boundary condition. The schematic of the boundary condition-1 is shown in the figure 3.5(a).

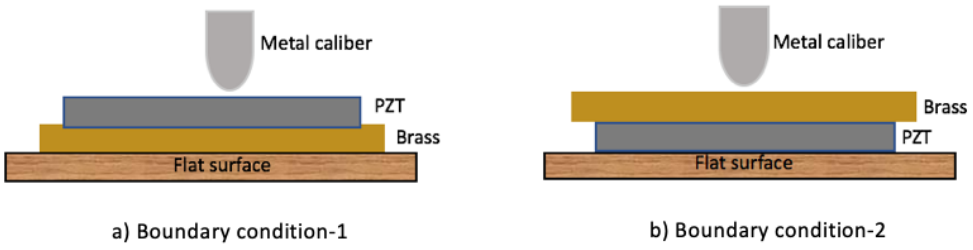

Figure 3.5: (a) Schematic representation of boundary condition-1. (b) Schematic representation of boundary condition-2

3.2.2 Boundary condition-2

Here in this boundary condition-2, no support is introduced. The piezoelectric buzzer is made to rest on the rigid flat surface with brass layer on the top position making a concentrated contact with the metal caliber of the piezometer and the PZT layer is in the bottom position resting on the rigid flat surface. The bending of the piezo buzzer structure is also not possible in this boundary condition-2. The schematic of the boundary condition-2 is shown in the figure 3.5(b).

3.2.3 Boundary condition-3

In the boundary condition-3, the piezoelectric buzzer is supported continuously by the ring support in order to induce bending in the piezo buzzer structure. The PZT layer is made to be on the top position and the brass layer is in the bottom position. The radius of the ring is made to match exactly with the radius of the PZT layer (a=0.013 m). Therefore the spherical Berlincourt metal caliber/indentator of the piezometer system makes a concentrated contact on the PZT layer, which in turn subjects the PZT layer to a compression loading condition and the brass plate to a tensile loading condition. The schematic of the boundary condition-3 is shown in the figure 3.6(a).

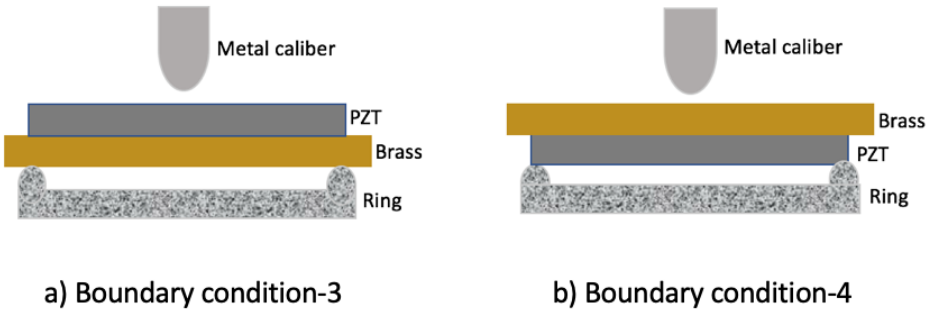

Figure 3.6: (a) Schematic representation of boundary condition-3. (b) Schematic representation of boundary condition-4

3.2.4 Boundary condition-4

Here in this boundary condition-4, the piezoelectric buzzer is supported continuously by the ring support. But the brass layer is on the top position to make a concentrated contact with the Berlincourt metal caliber/indentor of the piezometer system and the PZT layer is in the bottom position making a supporting contact with the ring. Therefore the brass

plate is subjected to compression loading condition which in turn makes the PZT layer to the tensile loading condition. The schematic of the boundary condition-4 is shown in the figure 3.6(b).

3.3 Working principle and procedure for mechanical testing

The main purpose of performing the mechanical tests is to determine the maximum load bearing capacity for the PZT layer of the piezoelectric buzzer when subjected to loading in four different boundary conditions.

In boundary condition 3 and 4, the piezoelectric buzzer is supported on the ring and it subjects the piezoelectric buzzer to pure bending. This type of loading creates a biaxial stress state on piezo buzzer structure, which is therefore same as the the specification of ball-on-the-ring tests procedure. Hence ball-on-the-ring test is performed to determine the maximum biaxial load for the PZT layer of the piezoelectric buzzer in the boundary condition 3 and 4.

In boundary condition 1 and 2, the piezoelectric buzzer is subjected to uniaxial compression and there is no bending involved, which is therefore same as the specification of the uniaxial compression testing procedure. Hence uniaxial compression test is performed to determine the maximum load bearing capacity for the PZT layer of the piezoelectric buzzer in the boundary condition 1 and 2.

3.3.1 Ball-on-the-ring tests

One of the widely used mechanical test to determine the maximum biaxial load for any bilayer or multilayer ceramic disc is ball-on-the-ring test. Dental ceramic structures are usually multilayered ceramics and uses biaxial flexural tests such as ball-on-ring bending test and ring-on-ring bending test to determine the maximum biaxial load and biaxial stress distribution to further study the rigidity of the ceramic structure [35].

The ball-on-the-ring test is standardised in ASTM C 1499-03 [36]. The analytical solutions available now for the ball-on-ring test cannot be used for non-linear behaviour (plastic behaviour). Since ceramics are brittle materials, the fracture of the material starts at the end of the elastic regime. Therefore this test can be more reliable to determine the end of the elastic limit or the beginning of the fracture in the ceramic material used [37].

Figure 3.7: Experimental setup for Ball-on-the-Ring

The set-up for the ball-on-the-ring test is shown in the figure 3.7. An Instron 5500R is used to perform the ball-on-the-ring test. This instrument consists of upper and the lower fixture. A 2525-806 Instron load cell is used for this experiment and this load cell is connected to the upper fixture, which has the capacity to measure a load of 1 kN. The load is applied on the piezoelectric buzzer through the ball connected via metal rod mounted on the load cell with the radius of b=0.004 m. The ball used to transfer the load from the load cell to the piezoelectric buzzer is shown in the figure 3.8.

The piezoelectric buzzer supported with the ring is placed on the lower fixture of the instrument. The displacement of the lower fixture, which is operated by lead-screw mechanism with respect to the load applied is determined. Constant displacement rate of 0.001m/s is maintained to perform the test until the fracture of the PZT layer in the piezoelectric buzzer. Instron bluehill-2 material testing software is an inbuilt software used to collect the data for the displacement as a function of the load applied on the piezoelectric buzzer supported with the ring. The experiment is conducted for the boundary condition 3 & 4 and the data are collected with the help of this software. The strain on the piezoelectric buzzer for the load applied is not measured in our experiments. The strain on the piezoelectric buzzer can be measured by connecting the strain gauge to the sample.

Figure 3.8: The Ball of radius 0.004m used for transferring the load from load cell to piezoelectric buzzer

3.3.2 Uniaxial compression test

The uniaxial compression test is used to determine the maximum load bearing capacity of the PZT layer in the piezoelectric buzzer. The uniaxial compression test is standardised in ASTM C1424 [38]. The compression test is also performed in the same Instron 5500R tensile machine. But the ring support is removed and the piezoelectric buzzer is made to rest on the rigid flat surface of the lower fixture. The test is performed by maintaining the constant displacement rate of 0.001m/s. The compression test is conducted for the boundary condition 1 and 2 and the displacement as a function of load applied on the piezoelectric buzzer is measured using the Instron bluehill-2.

Chapter 4

Results and discussion

The results section will be subdivided into 4 parts.

- Experimentally measured electrical output: stored energy
- Experimental results for the mechanical tests to determine maximum load bearing capacity.
- Analytically calculated mechanical input: elastic strain energy
- Comparison between the calculated mechanical input and stored electrical output.

4.1 Experimentally measured electrical output: stored energy, U (J)

The electrical output: stored energy for the piezoelectric buzzer tested in four different boundary conditions with 3 different static loadings (10 N,11.4 N and 13.4 N) is measured using the piezometer system. The working principle and the procedure to extract the data from the piezometer system are described in the chapter 3.

The comparison of the elctrical output: stored energy in the PZT layer of the piezoelectric buzzer for 4 different boundary conditions with the static load of 10 N is shown in the figure 4.1. The electrical output comparison for different boundary conditions with the increasing static loads are shown in the figure 4.2 and 4.3 respectively. First we shall discuss the electrical output: stored energy comparison for the static load of 10 N. The graph is plotted for the change in the electrical output: stored energy,(U) with respect to the force (N) applied. (the force applied is a summation of the pre-static load due to the offset voltage ($V_{DC} \times 2$), static load exerted by the voice coil(1.4 N) and the input quasi static load applied by varying the amplitude of sinusoidal wave frequency.

If we say 1 N is applied for the static load of 10 N, then the actual applied force will be 11 N after including all the pre-static load. For the static load of 11.4 N, it will be 12.4 N and 14.4 N for the static load of 13.4 N.

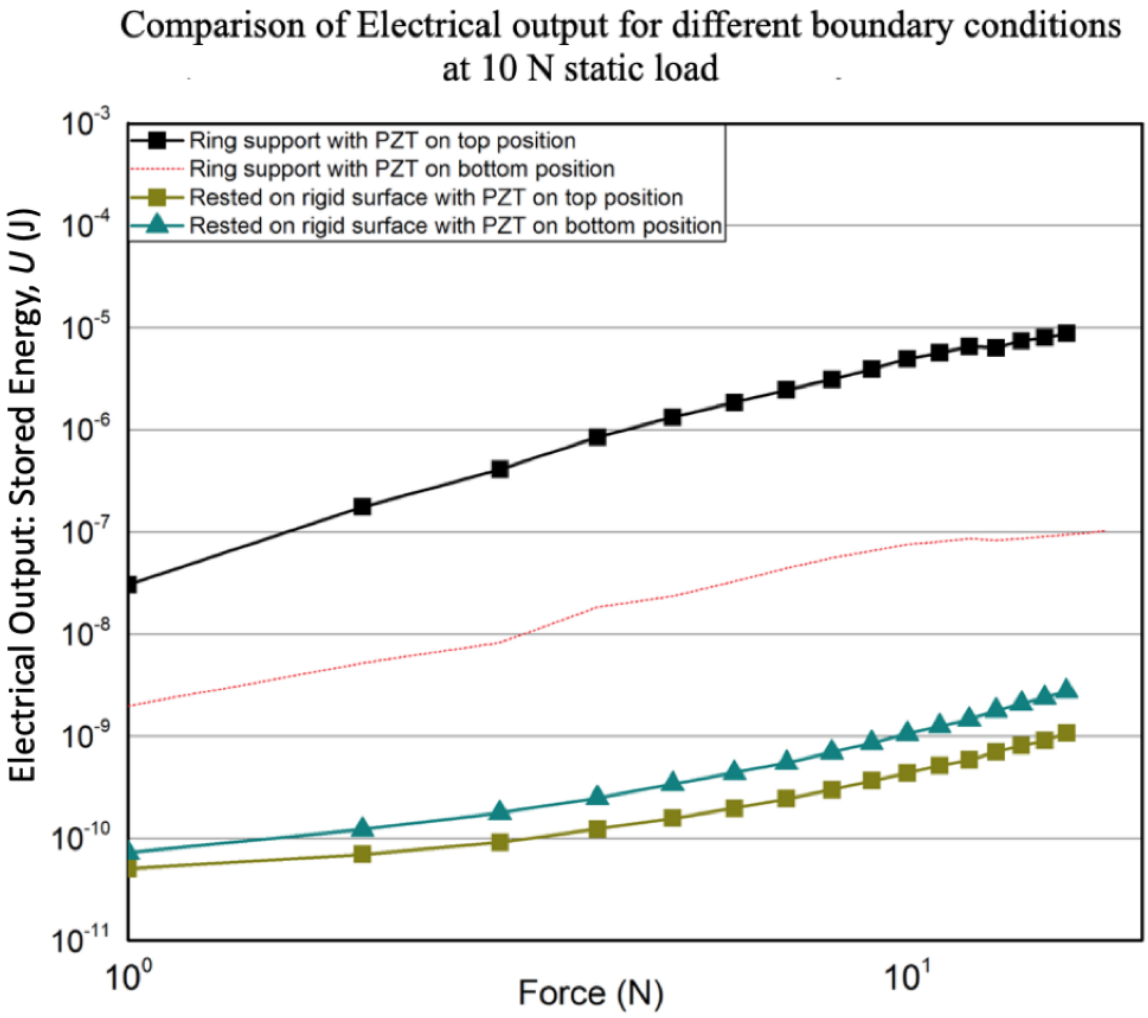

Figure 4.1: Comparison of stored electrical output for different boundary conditions at 10 N static load

It is evident from the figure 4.1, that the configuration of boundary condition-1 (piezoelectric buzzer placed on a rigid surface with PZT layer on the top position) has the least stored electrical energy. In the case of the boundary condition-2 (piezoelectric buzzer placed on a rigid surface with PZT layer on the bottom position), it shows a moderate increase in storing the electrical energy when compared to boundary condition-1.

By introducing the ring support for the piezoelectric buzzer to induce bending shows an immense increase in storing the electrical energy in the PZT layer and it can be seen that the boundary condition-3 (piezoelectric buzzer is supported by the ring with PZT layer on the top position) shows almost three order of magnitude higher stored electrical energy when compared to boundary condition-1 and 2.

The configuration of the boundary condition-4 (piezoelectric buzzer is supported by the ring with PZT layer on the bottom position) induces about an order of less stored electrical energy than the boundary condition-3. Also the trend for the boundary condition-4 shows a non-linear behaviour ,as it can be seen from the red curve in figure 4.1. The reason for this non-linear behaviour of stored electrical energy with respect to the load applied becomes understandable when explaining the analytically calculated mechanical input: elastic strain energy for the boundary condition-4 and the results for mechanical testing.

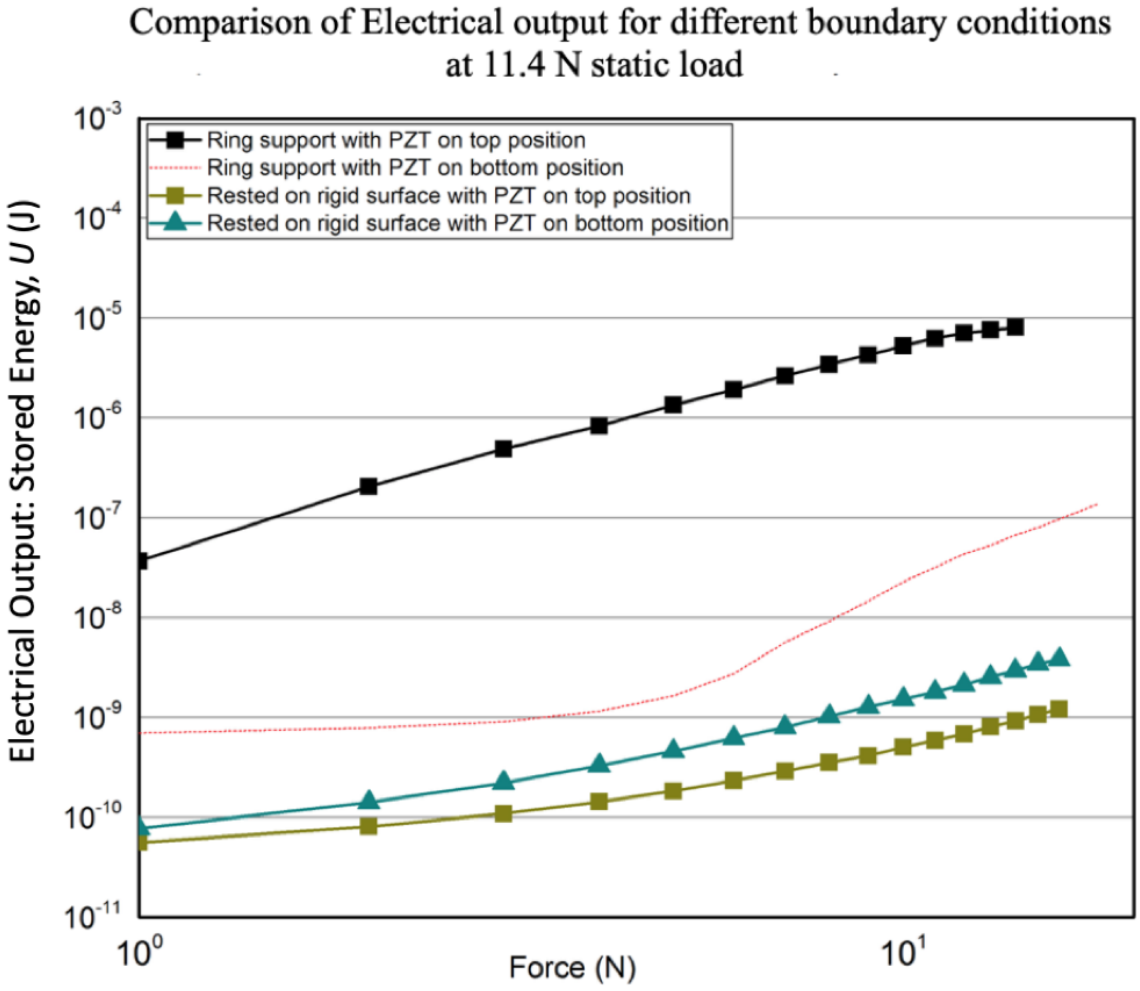

Figure 4.2: Comparison of stored electrical output for different boundary conditions at 11.4 N static load

The change in electrical output: stored energy for all the boundary conditions when increasing the pre-static load are studied. The static load is increased to 11.4 N and 13.4 N.

The comparison of the electrical output: stored energy for different boundary conditions with the static load of 11.4 N and 13.4 N are shown in the figure 4.2 and 4.3.

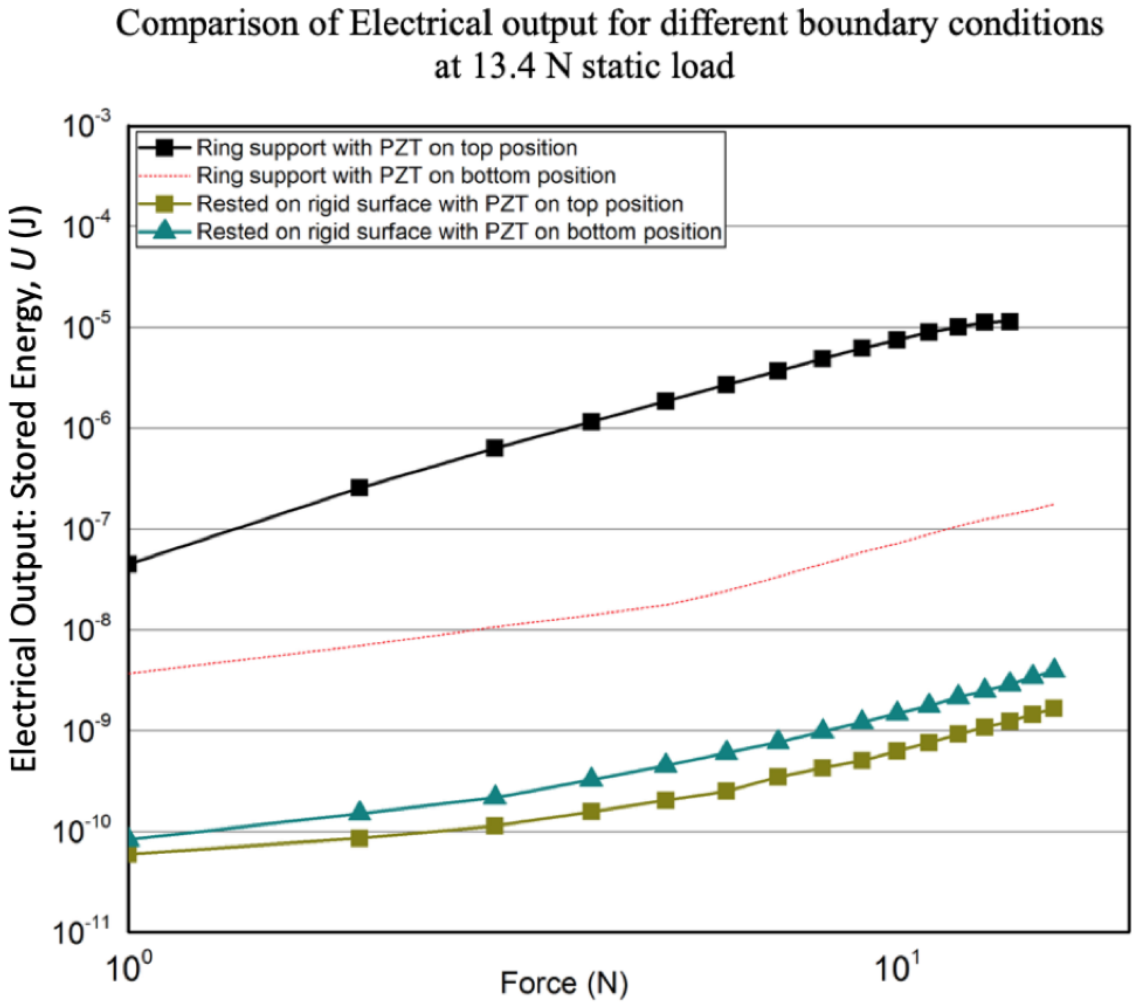

Figure 4.3: Comparison of stored electrical output for different boundary conditions at 13.4 N static load

The same trend (Boundary condition-3 > Boundary condition-4 > Boundary condition-2 > Boundary condition-1) as in the first measurement with 10 N static loading is repeated after increasing the static load to 11.4 N and 13.4 N. Thus increasing the offset DC voltage, results in increasing the pre-static load applied on the piezoelectric material. This increased pre-static load results in increasing the electrical output: stored energy in the piezoelectric buzzer in all four boundary conditions.

When comparing the results obtained for the electrical output: stored energy, U (J) with the results from [17], we can understand that the stored electrical output energy obtained

from the clamped disc condition in [17] is in good match with the electrical output obtained from the boundary condition-1 and 2. The range for the stored electrical output for clamped disc in [17] is from 1×10^{-11} J to 1×10^{-09} J for the increasing quasi static load upto 10 N. The range we obtained for the electrical output in our research for the boundary condition-1 and 2 is between 1×10^{-11} J to 1×10^{-09} J for the increasing quasi static load upto 10 N load applied. Also we know from [17] that changing the shape of the PZT plate from circular disc to rectangular plate has no effect in influencing the electrical output in clamped condition.

In the figure 2.5, unimorph cantilever configuration 4:1 (the length is 4 times its width) yields electrical output ranging from 1×10^{-6} J to 1×10^{-4} J for the increasing load upto 10 N, which is about 5 order of magnitude higher than the clamped condition of the disc. In our case, boundary condition-3 induces bending to the bilayer disc structure. The electrical output from this configuration stores electrical output ranging from 1×10^{-7} J to 1×10^{-05} J for the increasing quasi static load upto 10 N. This is about 1 order of magnitude range lesser than the electrical output obtained from unimorph cantilever configuration. Therefore, the unimorph cantilever configuration stores higher electrical output: stored energy than the bilayer piezobuzzer subjected to bending supported by the ring.

The effect of increasing the pre-static load on the electrical output for the boundary conditions- 1,2 and 3 is shown in Appendix A.1.

4.2 Experimental results for the mechanical tests

4.2.1 Uniaxial compression test for the boundary condition-1 & 2

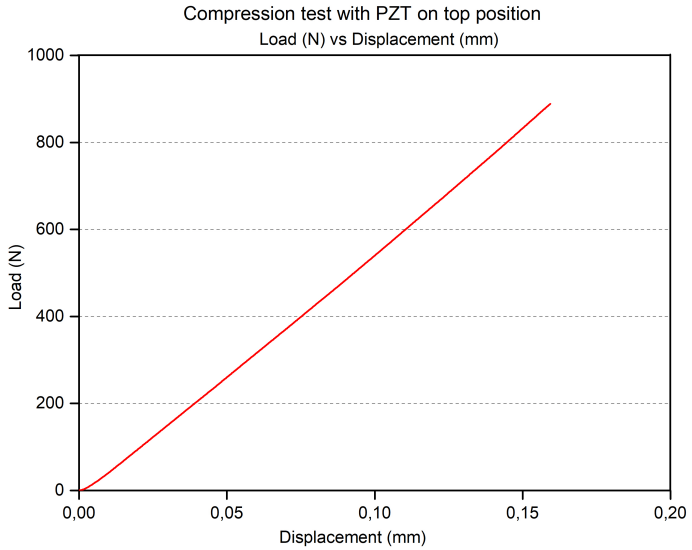

Figure 4.4: Load (N) vs Displacement (mm) curve for the boundary condition-1

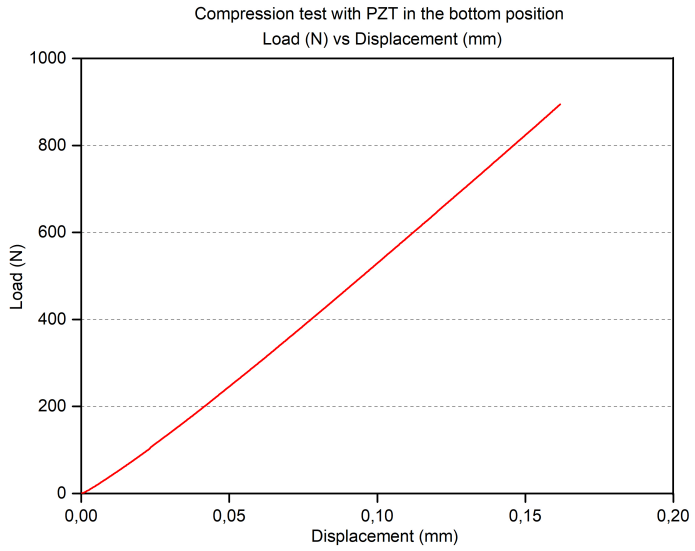

Figure 4.5: Load (N) vs Displacement (mm) curve for the boundary condition-2

From the figure 4.4, the Load (N) vs Displacement (mm) curve for the boundary condition-1 is determined using the uniaxial compression test. The displacement of the piezo buzzer is linear with the force applied. The full capacity of 1 kN is applied by the load cell on to the piezobuzzer structure and there is no fluctuation in the trend. This shows that piezobuzzer structure when subjected to boundary condition-1 type loading produces no fracture in the structure.

From the figure 4.5 , the Load (N) vs Displacement (mm) curve for the boundary condition-2 is determined using the uniaxial compression testing. Here in this boundary condition-2 , the PZT layer is on the bottom position and the brass layer is in direct contact with the loading ball. The piezo structure is made to rest on the flat rigid surface. No fluctuation in the trend is observed until the application of 1 kN for the boundary condition-2. This shows that piezobuzzer structure subjected to boundary condition-2 type loading produces no fracture to the structure.

4.2.2 Ball-on-the-ring test

The ball-on-the-ring test is carried out to determine the critical load at which the fracture begins in the PZT layer of the piezo buzzer for boundary condition 3 and 4. The loading configuration for the boundary condition 3 and 4 are same as that of the ball-on-the-ring test loading configuration.

4.2.3 Ball-on-the-ring test for the boundary condition-3

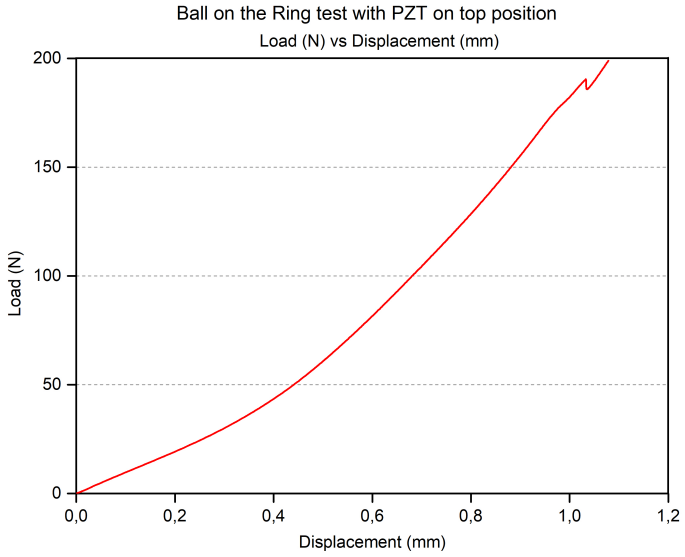

Figure 4.6: Load (N) vs Displacement (mm) curve for boundary condition-3

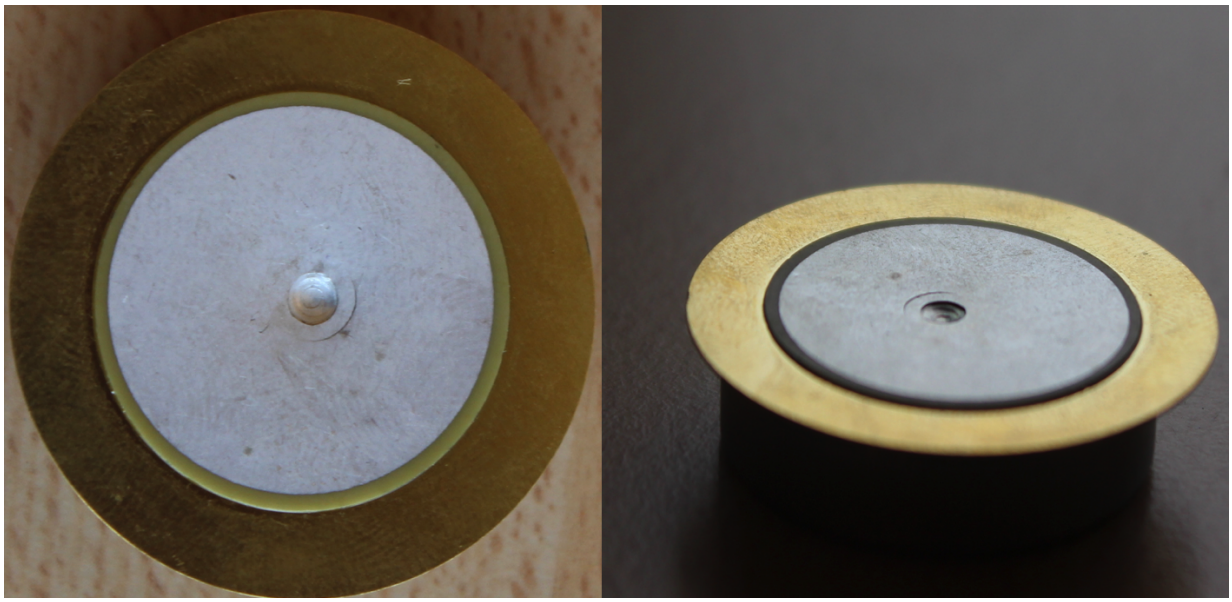

Figure 4.7: Permanent indentation of the ball on the PZT layer for boundary condition-3

The first experiment with the ball-on-the-ring test replicates the boundary condition-3, with the brass layer of the piezobuzzer structure is subjected to tensile loading and the PZT layer of the piezobuzzer which makes a concentrated contact with the ball is subjected to compressive loading condition.

It is clearly visible from the figure 4.6 that the displacement curve is continuous with the load applied until 180 N. The disruption in the continuous line is observed at 180 N. The critical load of 180 N is required to cause fracture in the PZT layer of the piezoelectric buzzer for the boundary condition-3. The piezoelectric buzzer sample used for this test shows a permanent indentation mark of the ball at the point of contact on the PZT layer for the applied load of 180 N.

4.2.4 Ball-on-the-ring test for boundary condition-4

The second experiment with the ball-on-the-ring test replicates the boundary condition-4, with the PZT layer of the piezoelectric buzzer is subjected to tensile loading because the PZT layer is placed at the bottom position and the brass layer makes a direct contact with the loading ball, which subjects the brass layer to a compressive loading.

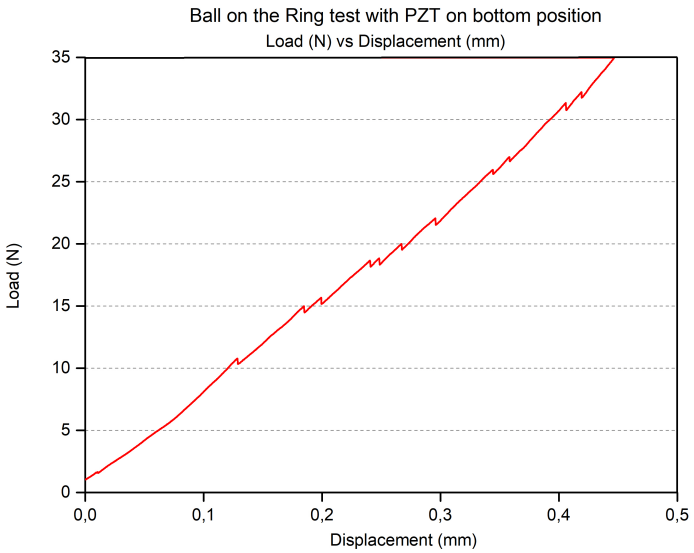

Figure 4.8: Load (N) vs Displacement (mm) curve for the boundary condition-4

As it can be seen from the figure 4.8 that the disruption in the curve starts at the force of 10 N, which will be the critical tensile force required to cause the fracture in the PZT layer of the piezoelectric buzzer loaded in the boundary condition-4. Since we knew, applying 1 N in the piezometer system would superimpose an additional pre-static load induced by the voice coil and by the DC offset voltage. This indicates that input of quasi static load of 1 N in 10 N, 11.4 N and 13.4 N pre-static load would result in applying 11 N, 12.4 N and 14.4 N respectively, which means more than 10 N is applied every time. This led to fracture of the PZT layer at the very first execution of the applied quasi static-force. Further loading of the piezoelectric buzzer in this boundary condition would result in the severe fracture of the PZT layer microscopically.

The cracks in the PZT layer are not visible visually. The capacitance of the piezoelectric buzzer before the experiment is measured to be 34 nF. The capacitance of the piezoelectric buzzer after subjecting to the ball-on-the-ring experiment for the boundary condition-2 showed a value of 22 nF, which is 35 percent decrease in the capacitance value after the experiment. Therefore the change in the capacitance of the PZT layer is observed and it confirms it might be due to the presence of internal cracks.

From the above experiments, it can be concluded that the piezobuzzer structure when subjected to uniaxial compression test can withstand higher load without fracture because there is no bending of the structure involved while loading.

Boundary condition	**Summary**
Boundary condition-1	No fracture is observed in PZT layer until 1 kN
Boundary condition-2	No fracture is observed in PZT layer until 1 kN
Boundary condition-3	Maximum load bearing capacity for the PZT layer is 180 N
Boundary condition-4	Maximum load bearing capacity for the PZT layer is 10 N

Table 4.1: Summary of the maximum load bearing capacity of PZT layer in different boundary conditions

4.3 Calculated mechanical input: elastic strain energy comparision for different boundary conditions

The mechanical input: elastic strain energy for all the boundary conditions are calculated analytically. The analytical approach for the boundary condition 1 and 2 are completely different from the analytical approach of boundary condition 3 and 4. The Saint Venant's principle is used for the boundary conditions 3 and 4 to determine the mechanical input: elastic strain energy. The effect of bending is determined to be a plate thickness away from the point of application of the load.

The approach used for calculating mechanical input: elastic strain energy for the boundary condition 1 and 2 is by using the clamped condition formula to find the mechanical input: elastic strain energy.

Let us begin with the method used for solving the mechanical input: elastic strain energy for the boundary condition-1 analytically.

4.3.1 Boundary condition-1

For the boundary condition-1, the piezo buzzer is made to rest on a rigid surface. The PZT layer is on the top position making a concentrated contact with the metal caliber. So the PZT layer itself feels the brass layer as a rigid surface. This condition is similar to that of the compression of clamped circular plate condition and the formula for this condition is obtained from [17].

$$U = \frac{F^2 t}{2AE_{PZT}} \tag{4.1}$$

where F is the applied force, A is the area of PZT and E_{PZT} is the Young's modulus for PZT obtained from [39]. The mechanical input: elastic strain energy (U) is calculated from the equation 4.1.

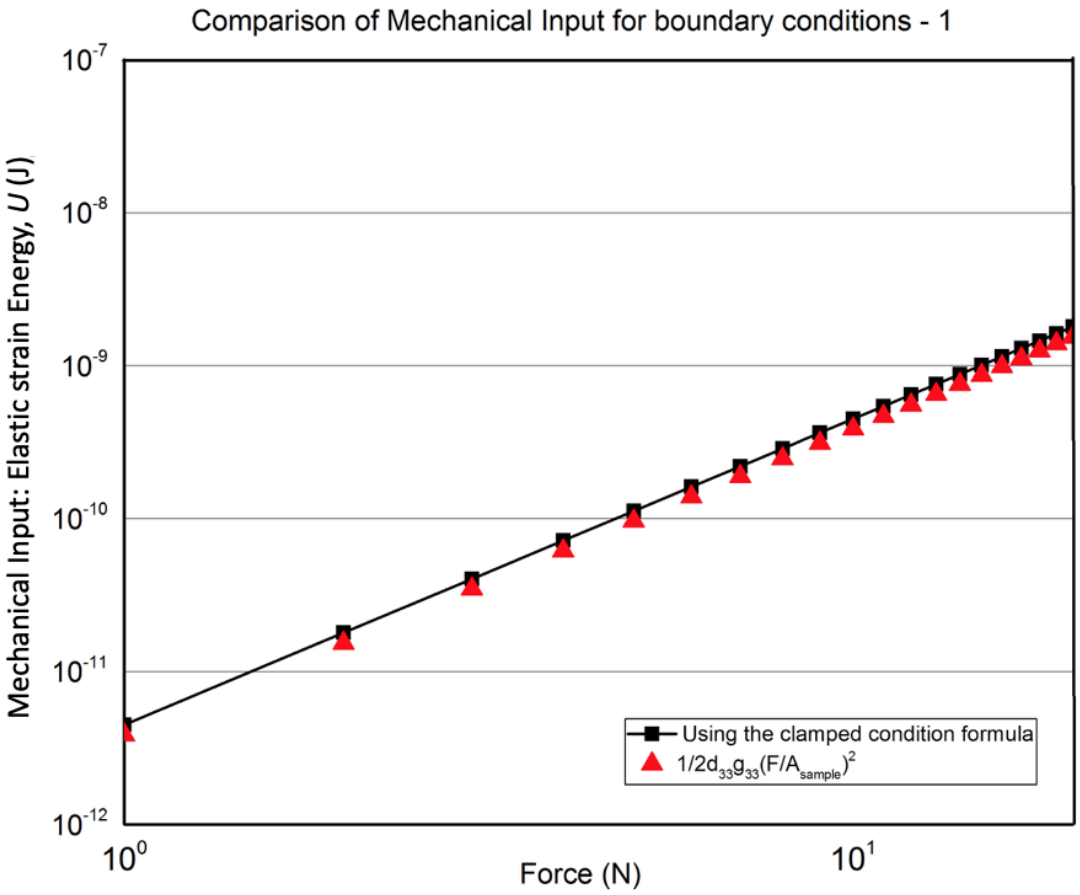

Figure 4.9: Mechanical input: elastic strain energy comparison with $1/2 \times d_{33}g_{33}(F/A)^2$ for boundary condition-1

The approach using the clamped condition formula makes a good agreement with the curve calculated using $1/2 \times d_{33}g_{33}(F/A)^2$.

4.3.2 Boundary condition-2

Here in this boundary condition-2, the PZT layer is in the bottom position and the brass layer makes a concentrated contact with the metal caliber. The force from the metal caliber is transferred through the brass plate.

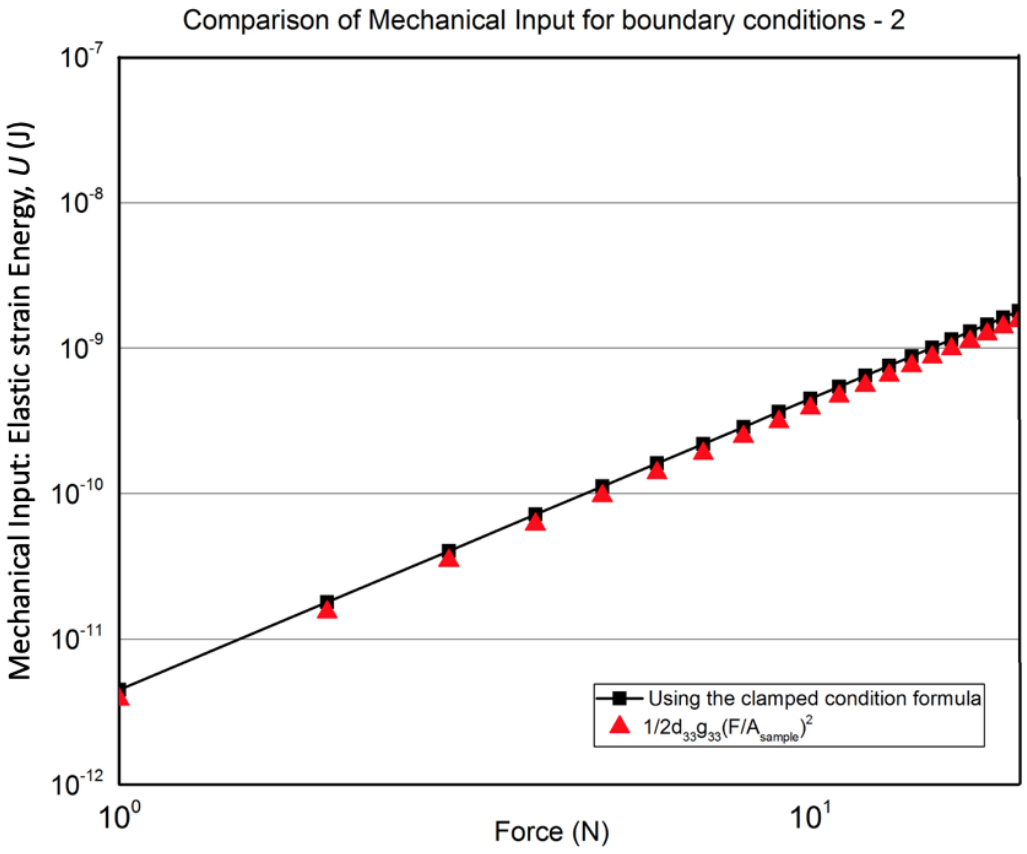

Figure 4.10: Mechanical input: elastic strain energy comparison with $1/2\times d_{33}g_{33}(F/A)^2$ for boundary condition-2

The mechanical input: elastic strain energy for the boundary condition-2 is calculated using the equation 4.1. The approach using the clamped condition formula makes a good agreement with the curve calculated using $1/2\times d_{33}g_{33}(F/A)^2$.

4.3.3 Boundary condition-3

Here in this boundary condition, ring support is introduced to the piezobuzzer to induce bending. The analytical model from [35] is used to determine the thickness averaged $\overline{\sigma}_r$ and $\overline{\sigma}_\theta$ for the bilayer piezobuzzer loaded with the ring support. The obtained $\overline{\sigma}_r$ and $\overline{\sigma}_\theta$ will be used to determine the mechanical input: elastic strain energy for the boundary condition-3. In this boundary condition, PZT is in the top position and the stress distribution related

to the top PZT layer is the area of our interest. Bending of the circular plates are discussed in various paper [40], [41], [42]. Cylindrical coordinates r, θ and z are used in this analysis.

The values for the PZT and Brass material properties are taken from [39] [43]

Material Properties	**Parameter**
Young's Modulus of PZT (E_{PZT})	63 GPa
Young's Modulus of Brass (E_{brass})	110 GPa
Poison's ratio of the PZT (μ_{PZT})	0.31
Poison's ratio of the brass layer (μ_{brass})	0.357

Table 4.2: PZT and Brass material Properties and their Parameter

The schematic for the geometrical dimension of the piezobuzzer loaded in the boundary condition-3 is shown in the figure 4.11:

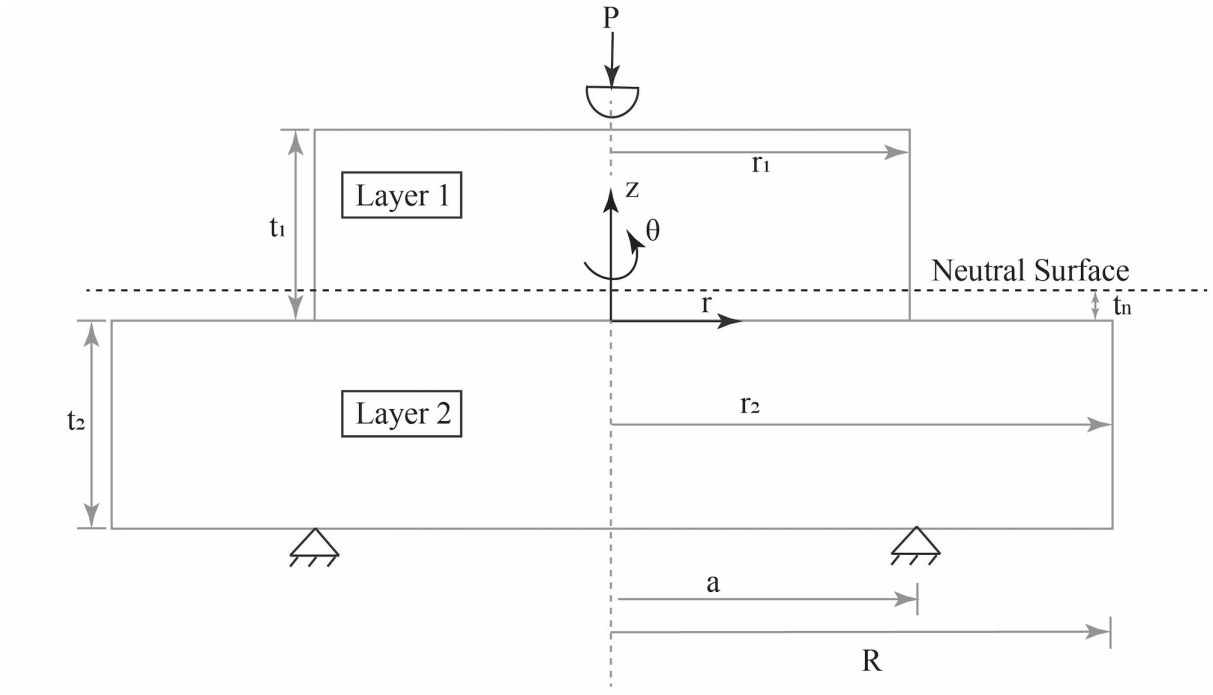

Figure 4.11: Schematic representation of the Boundary condition-3

Geometrical Parameters	Dimension
Thickness of the PZT layer (t_{PZT})	0.0003 m
Thickness of the brass layer (t_{brass})	0.0002 m
Radius of the PZT layer (r_{PZT})	0.013 m
Radius of the Brass layer (r_{brass})	0.017 m
Radius of the ring (a)	0.013 m
Edge of the plate (R)	0.017 m

Table 4.3: Geometrical Dimension and their parameter

Here in this boundary condition-3, the PZT material in the top position will be the layer-1 and its respective dimension and material properties parameters used in the equations is denoted with subscript 1. The brass material is in the bottom position and it will be layer-2. The respective material properties and dimensional parameters of brass are denoted with subscript 2.

The stress distribution for thin bi-layer discs subjected to ball-on-ring test is given by [35]. In their research, the analytical expression for bilayer stresses are derived starting from the stress distribution for monolayer discs subjected to pure bending under small defection. Through the thickness averaged radial stress $\overline{\sigma}_{r_1}$ and hoop stress $\overline{\sigma}_{\theta_1}$ for layer 1 (z=t_n to t_1) in the bilayer disc is given for two different regions along the radial direction.

The thickness averaged hoop stress ($\overline{\sigma}_{\theta 1}$) and thickness averaged radial stress($\overline{\sigma}_{r1}$) for r $\leq$ b is same.

$$\begin{aligned}\overline{\sigma}_{r1} = \overline{\sigma}_{\theta 1} = &-\frac{3F_1P(1+\nu)(t_1-2t_n)}{4\pi(t_1+t_2)^3} \\ &\times\left[1+2\ln\left(\frac{a}{b}\right)+\frac{1-\nu}{1+\nu}\left(1-\frac{b^2}{2a^2}\right)\frac{a^2}{R^2}\right](for\ r\leq b)\end{aligned} \tag{4.2}$$

The thickness averaged radial stress($\overline{\sigma}_{r1}$) for r > b is given as

$$\begin{aligned}\overline{\sigma}_{r1} = &-\frac{3F_1P(1+\nu)(t_1-2t_n)}{4\pi(t_1+t_2)^3} \\ &\times\left[2\ln\left(\frac{a}{r}\right)+\frac{1-\nu}{2(1+\nu)}\left(1-\frac{r^2}{a^2}\right)\frac{a^2}{r^2}\frac{b^2}{R^2}\right](for\ r>b)\end{aligned} \tag{4.3}$$

The thickness averaged hoop stress($\overline{\sigma}_{\theta 1}$) for r > b is given as

$$\begin{aligned}\overline{\sigma}_{\theta 1} = &-\frac{3F_1P(1+\nu)(t_1-2t_n)}{4\pi(t_1+t_2)^3} \\ &\times\left[2\ln\left(\frac{a}{r}\right)+\frac{1-\nu}{2(1+\nu)}\left(4-\frac{b^2}{r^2}\right)\frac{a^2}{R^2}\right](for\ r>b)\end{aligned} \tag{4.4}$$

where,

t_n : Neutral surface position

P : Applied load

ν : Effective Poisson's ratio

F : Flexural rigidity

a : Radius of the ring

r : Radial position

b : Hertzian contact radius

R : Edge of the piezobuzzer disc

σ_r : Radial stress

σ_θ : Hoop stress

The neutral surface position (t_n) is a plane that seperates the piezobuzzer into two section. The section above the neutral surface is in compression and the section below the neutral surface is in tensile. The neutral surface position (t_n) for this boundary condition is calculated using:

$$t_n = \frac{E_1 t_1^2 - E_2 t_2^2}{2(E_1 t_1 + E_2 t_2)}. \tag{4.5}$$

Since PZT is the layer 1, the flexural rigidity (F_1) for the layer-1 is given as

$$F_1 = \frac{E_1(E_1 t_1 + E_2 t_2)(t_1 + t_2)^3}{(E_1 t_1^2)^2 + (E_2 t_2^2)^2 + 2E_1 E_2 t_1 t_2(2t_1^2 + 2t_2^2 + 3t_1 t_2)}. \tag{4.6}$$

The Hertzian contact area radius (b) for the condition of stainless steel spherical caliber on the PZT surface can be calculated using [44]

$$b = \sqrt[3]{\frac{3RF\left[\frac{1-\nu_0^2}{E_0} + \frac{1-\nu_1^2}{E_1}\right]}{2}} \tag{4.7}$$

where, the Young's modulus of the stainless steel (E_0) is 203 GPa and its Poison's ratio is 0.275 [43].

The effective Poison's ratio for the Piezo buzzer is calculated according to: [35]

$$\nu = \frac{\nu_1 t_1 + \nu_2 t_2}{t_1 + t_2}. \tag{4.8}$$

Using the saint Venant's principle, the full effect of bending moment for the plate is experienced in the piezoelectric buzzer plate thickness away from hertzian contact radius by the application of the load [45] and it is shown in the figure 4.12. From the above equations, thickness averaged hoop stress ($\overline{\sigma}_{\theta_1}$)and thickness averaged radial stress ($\overline{\sigma}_{r_1}$) along the radial position from r=0 to r= b+0.0005 m can be found. The main contribution for bending for this boundary condition comes within the region from r=0 to r=b+0.0005 m, where b is the hertzian contact region and it is proportional to the load applied (P). The neutral surface position lies at t=1.55×10^{-5} m. The thickness region from t=1.55×10^{-5} m to t=0.0003 m is the PZT thickness region subjected to compressive loading and t=0 m to t=1.55×10^{-5} m thickness subjected to tensile. These region contributes to the mechanical input: elastic strain energy.

From the calculated hoop stress($\overline{\sigma}_{\theta_1}$) and radial stress($\overline{\sigma}_{r_1}$) within the radial region r=0 to r=b+0.0005 m and through the thickness region from t=0 m to t=0.0003 m for the boundary condition-3, the mechanical input: elastic strain energy can be calculated from following the respective steps.

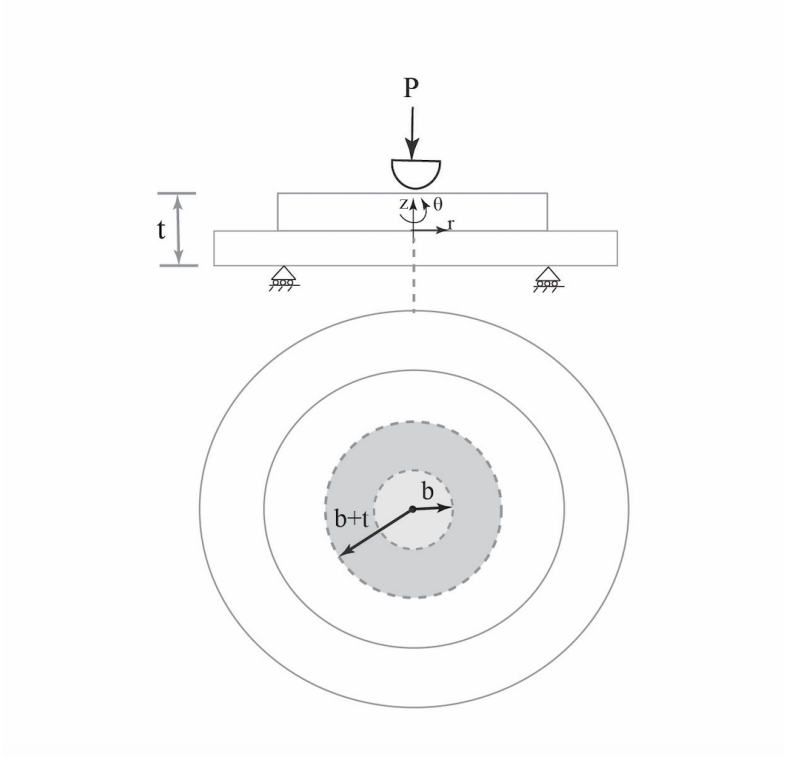

Figure 4.12: Schematic representation of the responsible bending region found using St.Venant's Principle

$$U_{r\leq b} = \int_0^{t_1}\int_0^{2\pi}\int_0^{b}(\overline{\sigma}_{r1}\overline{\epsilon}_{r1} + \overline{\sigma}_{\theta 1}\overline{\epsilon}_{\theta 1})\, r\, dr\, d\theta\, dz \quad (for\ r \leq b) \tag{4.9}$$

For the region r $\leq$ b, the mechanical input: strain energy, U (J) given in the equation 4.10 is calculated by using the thickness averaged stresses($\overline{\sigma}_{\theta_1}$, $\overline{\sigma}_{r_1}$) and strains ($\overline{\epsilon}_{r1}$,$\overline{\epsilon}_{\theta 1}$) with in that volume.

For the region r > b, the mechanical input, elastic strain energy, U (J) is given in the equation 4.11. Finally, U_{Total} is found, which will be the mechanical input: elastic strain energy for the PZT plate.

$$U_{r>b} = \int_0^{t_1} \int_0^{2\pi} \int_b^{(b+t)} \left(\frac{\overline{\sigma}_{r1} + \overline{\sigma}_{\theta 1}}{2}\right) \left(\frac{\overline{\epsilon}_{r1} + \overline{\epsilon}_{\theta 1}}{2}\right) r\, dr\, d\theta\, dz \quad (for\ r > b) \tag{4.10}$$

$$U_{Tot} = \frac{1}{2}(U_{r\leq b} + U_{r>b}) \tag{4.11}$$

The piezobuzzer used in our experiment is a thin flat plate. The stresses acting along the z-direction in thin flat plate is considered to be negligible. So this is a plane stress condition [46]. The thickness averaged hoop strain and radial strain relation with respect to the required stresses are calculated as follow:

$$\overline{\epsilon}_{r1} = \frac{1}{E_{PZT}} \left[\overline{\sigma}_{r1} - \nu_{PZT}\overline{\sigma}_{\theta 1}\right] \tag{4.12}$$

$$\overline{\epsilon}_{\theta 1} = \frac{1}{E_{PZT}} \left[\overline{\sigma}_{\theta 1} - \nu_{PZT}\overline{\sigma}_{r1}\right] \tag{4.13}$$

These integrations are carried out using the "integral function" in Matlab.

4.3.4 Boundary condition-4

For the boundary condition-4, we know that the brass plate is on the top position and the PZT layer is on the bottom position. The neutral surface position for this boundary condition-4 is found to be at $t_n = 8 \times 10^{-5}$ m, lies in the brass plate and subjecting the whole PZT layer in the tensile loading condition.

Here in this boundary condition-4, the PZT is in the bottom position and its respective dimensions and materials properties parameters are treated with the subscript-2. The brass plate is in the top position and its respective material properties and dimensional parameters are denoted with subscript-1.

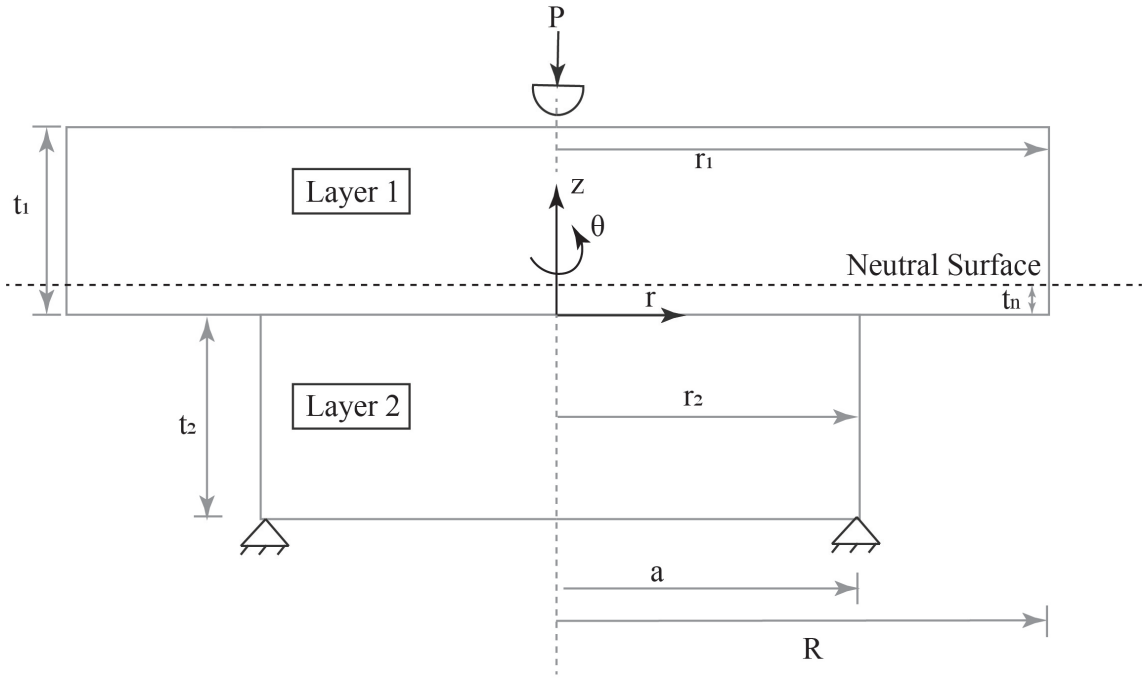

Figure 4.13: Schematic representation for the boundary condition-4

The main contribution for bending for this boundary condition comes within the region from r=0 to r=b+0005 m which is determined using St.Venant's Principle. The region from t=-0.0003 m to t=0 m is the responsible thickness region putting the PZT layer in the tensile loading condition. The modified thickness averaged radial stress and modified thickness averaged hoop stress is given in the equation 4.15, 4.16 and 4.17.

The averaged thickness hoop stress ($\overline{\sigma}_{\theta 2}$) and thickness averaged radial stress($\overline{\sigma}_{r2}$) for r $\leq$ b is same.

$$\begin{aligned}\overline{\sigma}_{r2} = \overline{\sigma}_{\theta 2} = & \frac{3F_2P(1+\nu)(t_2+2t_n)}{4\pi(t_1+t_2)^3} \\ & \times \left[1 + 2\ln\left(\frac{a}{b}\right) + \frac{1-\nu}{1+\nu}\left(1 - \frac{b^2}{2a^2}\right)\frac{a^2}{R^2}\right] (for\ r \leq b)\end{aligned} \tag{4.14}$$

The thickness averaged radial stress($\overline{\sigma}_{r2}$) for r > b is as follows.

$$\begin{aligned}\overline{\sigma}_{r2} = & \frac{3F_2P(1+\nu)(t_2+2t_n)}{4\pi(t_1+t_2)^3} \\ & \times \left[2\ln\left(\frac{a}{r}\right) + \frac{1-\nu}{2(1+\nu)}\left(1 - \frac{r^2}{a^2}\right)\frac{a^2}{r^2}\frac{b^2}{R^2}\right] (for\ r > b)\end{aligned} \tag{4.15}$$

The thickness averaged hoop stress($\overline{\sigma}_{r2}$) for r > b is as follows

$$\begin{aligned}\overline{\sigma}_{\theta 2} = & \frac{3F_2P(1+\nu)(t_2+2t_n)}{4\pi(t_1+t_2)^3} \\ & \times \left[2\ln\left(\frac{a}{r}\right) + \frac{1-\nu}{2(1+\nu)}\left(4-\frac{b^2}{r^2}\right)\frac{a^2}{R^2}\right](for\ r>b)\end{aligned} \tag{4.16}$$

The flexural rigidity,(F_2) for PZT in the layer-2 situation is

$$F_2 = \frac{E_2^*(E_1^*t_1 + E_2^*t_2)(t_1+t_2)^3}{(E_1^*t_1^2)^2 + (E_2^*t_2^2)^2 + 2E_1^*E_2^*t_1t_2(2t_1^2+2t_2^2+3t_1t_2)}. \tag{4.17}$$

The hertzian contact area radius (b) for the condition of stainless steel sphere on the Brass plate can be calculated using

$$b = \sqrt[3]{\frac{3RF\left[\frac{1-\nu_0^2}{E_0} + \frac{1-\nu_1^2}{E_1}\right]}{2}} \tag{4.18}$$

where, the Young's modulus (E_1) and the Poison's ratio (ν_1) of the brass is used.

After finding out the thickness averaged hoop stress and thickness averaged radial stress for two region in the boundary condition-4, the mechanical input: elastic strain energy is calculated by following the steps followed in the boundary condition-3. The "Integral function" in Matlab is used for solving the integration.

4.3.5 Final results for mechanical input: elastic strain energy, *U* (J)

The analytical methods mentioned in the section 4.3.1, 4.3.2, 4.3.3 and 4.3.4 are used to find the mechanical input: elastic strain energy for boundary conditions-1,2,3 and 4. The final results are compared and discussed in this section.

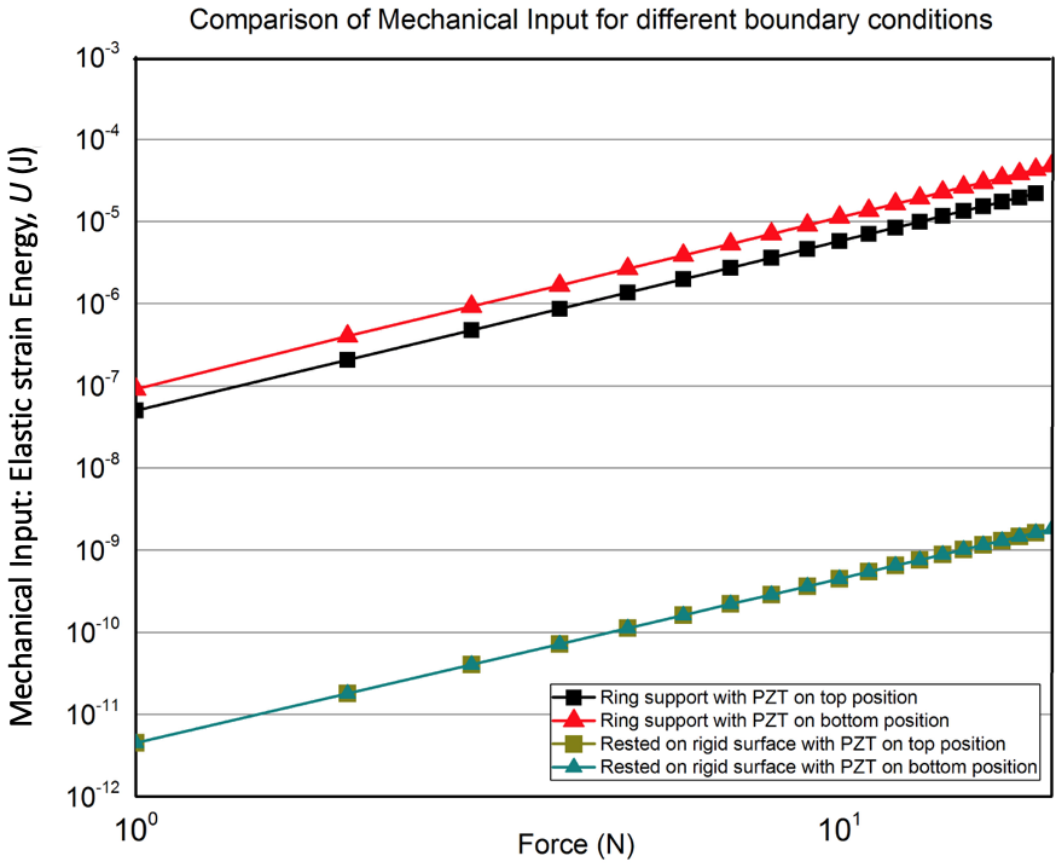

Figure 4.14: Comparison of mechanical input for different boundary conditions

As it can be seen from the figure 4.13, the mechanical boundary condition-4 with the ring support subjecting the PZT layer in the tensile loading condition, induces bending to the piezoelectric buzzer and maximises the stresses experienced in the PZT layer. The boundary condition-4 results in higher mechanical input: elastic strain energy than other boundary conditions.

Following the boundary condition-4, boundary condition-3 which is also supported with the ring but the PZT layer is in the compressive loading condition. This induces bending to the piezoelectric buzzer and maximises the stresses experienced in the PZT layer. The mechanical input energy experienced by the PZT layer in the boundary condition-3 is followed after the boundary condition-4.

The reason why the boundary condition-4 yields mechanical input energy higher than the boundary condition-3 is that the neutral surface position in the boundary condition-4 is positioned inside the brass plate, which in turn subject large volume of PZT layer to

tensile stresses. But in the case of boundary condition-3 the neutral surface position is placed inside the PZT layer and subjecting a limited volume of PZT to compression and larger volume of the piezobuzzer to tensile stresses. The position of the neutral surface can be clearly seen in the figure 4.11 and 4.13 for boundary condition 3 and 4 respectively.

The boundary condition-1 and 2, which experiences lower stresses due to the absence of bending during loading yields almost four order of magnitude lower elastic strain energy than the boundary condition 3 and 4. The mechanical input: elastic strain energy for the boundary condition-1 and 2 is calculated using the approach-1.

The thickness averaged radial and hoop stress stress distribution for the boundary condition-3 and 4 along the radial distance in the PZT layer for the applied load of 1 N and at their critical load (determined from the mechanical test experiment) are shown and discussed in Appendix A.3. Biaxial stress distribution along the radial distance determined using FEA analysis at 20 N and the analytically calculated method for the boundary condition-3 at 20 N is compared in the section A.2 of the Appendix chapter.

4.4 Comparison between the analytically calculated mechanical input and the experimentally obtained stored electrical output

Let us begin with the Boundary condition-3

4.4.1 Boundary condition-3

The figure 4.15 shows the comparison between the analytically calculated mechanical input: elastic strain energy and the electrical output:stored energy for the boundary condition-3 with the static load of 10 N.

As it can be seen from the figure 4.15 that the mechanical input and electrical output almost matches exactly for all the values of load applied, which means that all the applied mechanical input is converted as electrical output: stored energy for all the values of load. Increasing the static load does a small increase in the stored electrical output. The effect of increasing the static load on the stored electrical output is shown in the appendix.

In the case of the static load 13.5 N, the analytically predicted mechanical input is slightly under predicted than the stored electrical output.

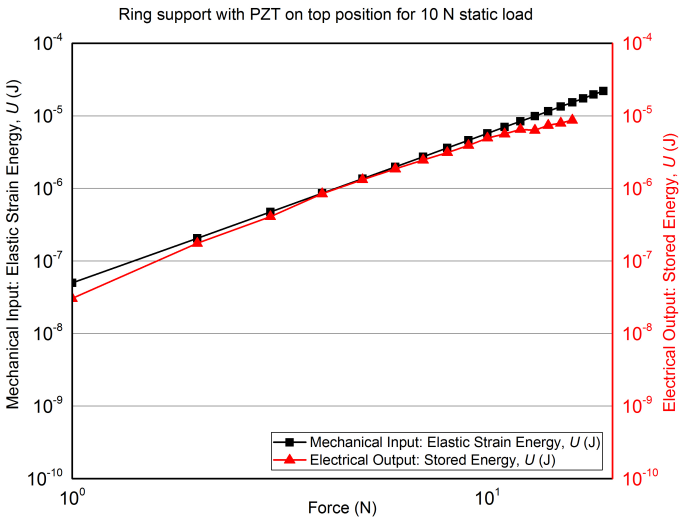

Figure 4.15: Comparison between the mechanical input and electrical output for the boundary condition-3 with the static load of 10 N

Figure 4.16 and figure 4.17 shows the comparison between the mechanical input and electrical output for the boundary condition-3 with the static load of 11.4 N and 13.4 N

respectively.

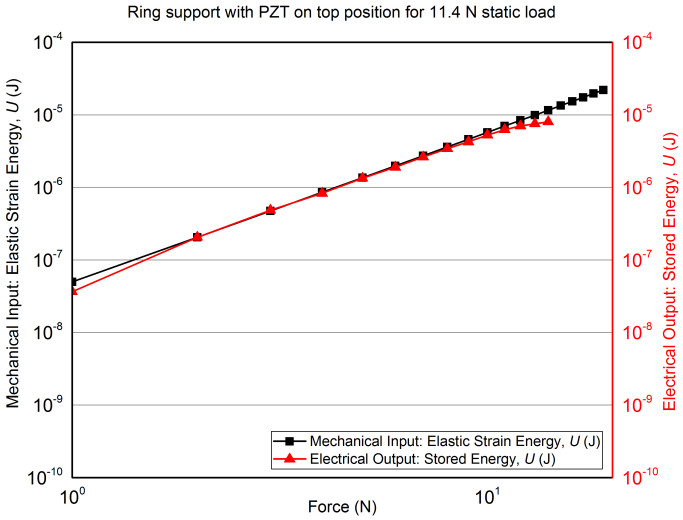

Figure 4.16: Comparison between the mechanical input and electrical output for the boundary condition-3 with the static load of 11.4 N

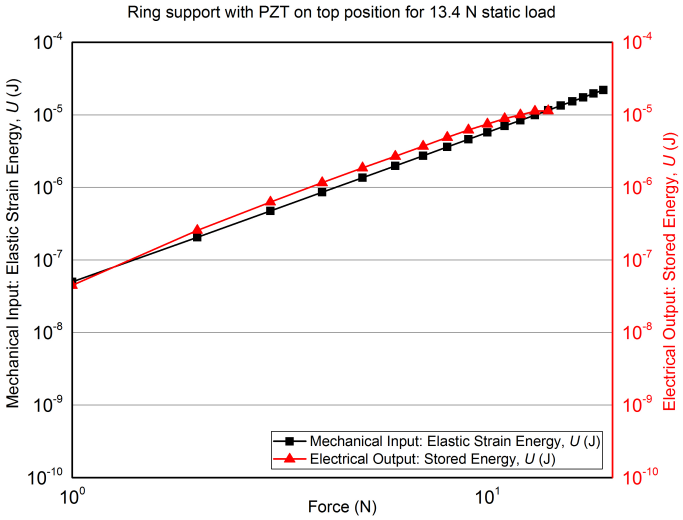

Figure 4.17: Comparison between the mechanical input and electrical output for the boundary condition-3 with the static load of 13.4 N

4.4.2 Boundary condition-4

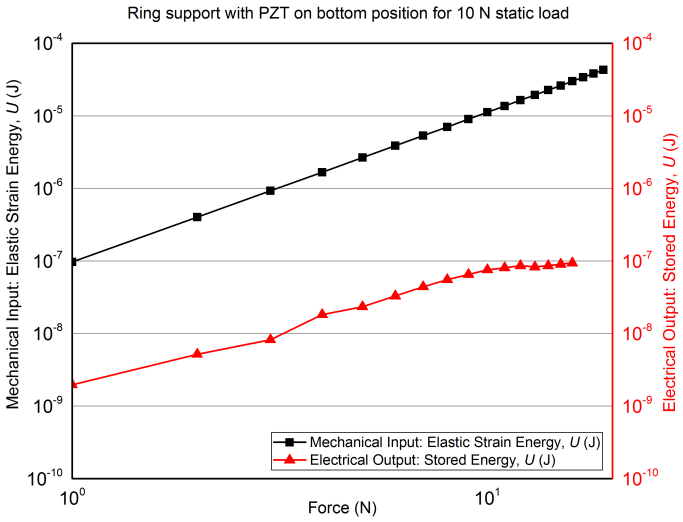

Figure 4.18: Comparison between the mechanical input and electrical output for the boundary condition-4 with the static load of 10 N

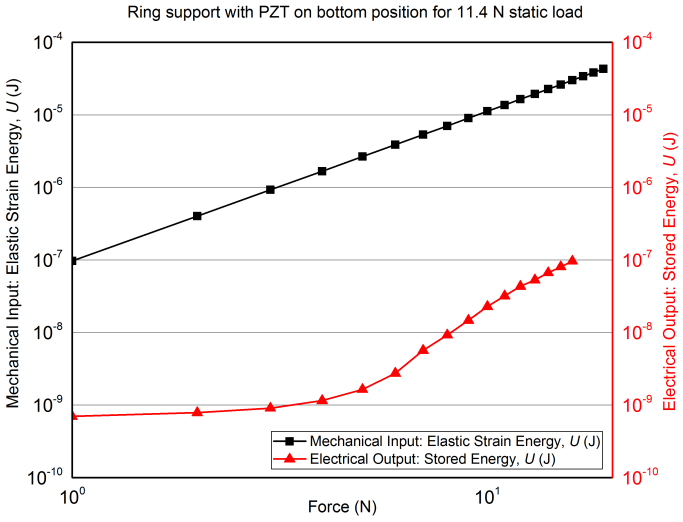

Figure 4.19: Comparison between the mechanical input and electrical output for the boundary condition-4 with the static load of 11.4 N

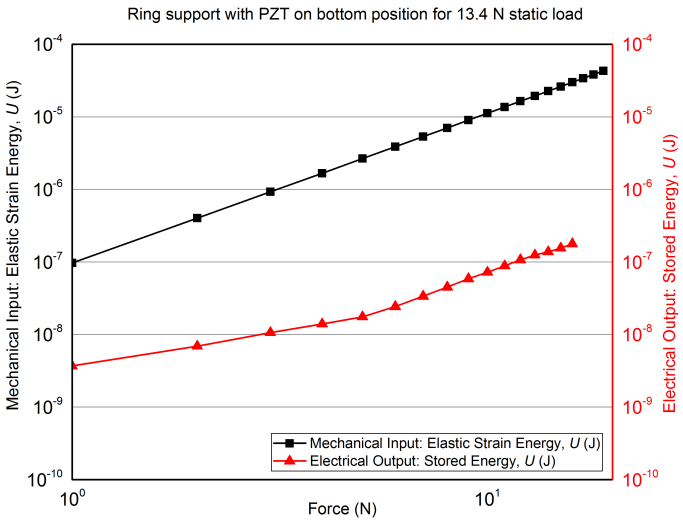

Figure 4.20: Comparison between the mechanical input and electrical output for the boundary condition-4 with the static load of 13.4 N

Figure 4.18 shows the comparison between the calculated mechanical input and the experimentally obtained electrical output for the boundary condition-4. Disparity with two order of magnitude can be seen from the figure 4.18 between the analytically predicted mechanical input: elastic strain energy experienced by the PZT layer and the experimentally obtained stored energy for all the values of load applied. The same pattern is obtained for the boundary condition-4 when increasing the static load from 11.4 N to 13.4 N is Shown in the figure 4.19 and 4.20.

The reason for this disparity in the boundary condition-4 for all the values of load applied can be understood from the figure 4.8. The load vs displacement curve obtained for ball-on-the-ring test replicating the boundary condition-4 shows explicitly that the PZT layer is fractured at the very first application of load because the PZT layer is subjected to a tensile loading condition. The fractured PZT layer must experience uneven distribution of stress. Also reduced capacitance value is observed in the PZT layer after the experiment. This confirms that subjecting PZT layer in tensile loading does not help in transducting the predicted mechanical input: elastic strain energy to the experimentally measured electrical output: stored energy, because of the fracture in the PZT layer at the very first application of load.

4.4.3 Boundary condition-1

The comparison between the mechanical input and the electrical output for the boundary condition-1 with the static load for 10 N is shown in the figure 4.21. The loading condition does not involves bending. The measured electrical output: stored energy is higher than the analytically calculated mechanical input: elastic strain energy. During the stored electrical output measurement the piezoelectric buzzer is placed over the Berlincourt metal caliber, which is not a flat rigid surface could the reason for this discrepancy because it might slightly induce bending in the piezoelectric buzzer. Therefore this results in measuring high electrical output: stored energy. Further study is needed to fully understand this discrepancy.

Figure 4.21: Comparison between the mechanical input and electrical output for the boundary condition-1 with the static load of 10 N

The same pattern for the comparison is obtained for the increased static load 11.4 N and 13.4 N. The comparison for the boundary condition-1 for the static load of 11.4 N and 13.4 N is shown in the figure 4.22 and 4.23.

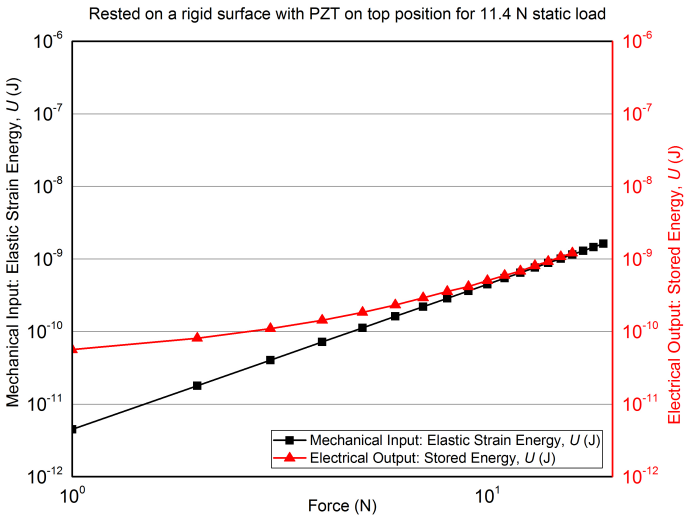

Figure 4.22: Comparison between the mechanical input and electrical output for the boundary condition-1 with the static load of 11.4 N

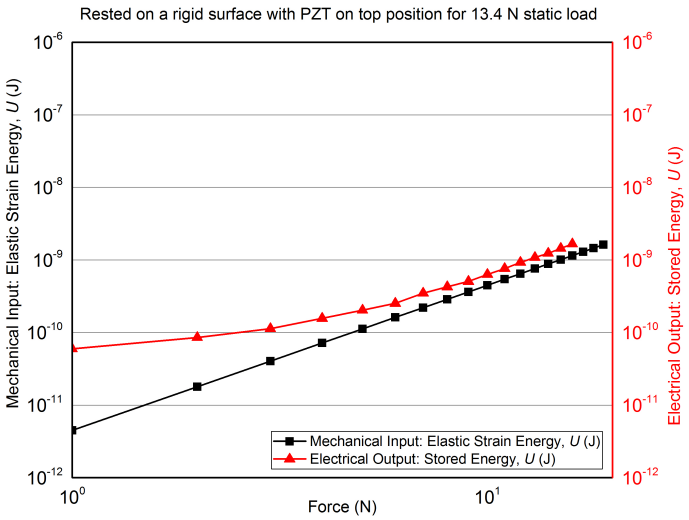

Figure 4.23: Comparison between the mechanical input and electrical output for the boundary condition-1 with the static load of 13.4 N

4.4.4 Boundary condition-2

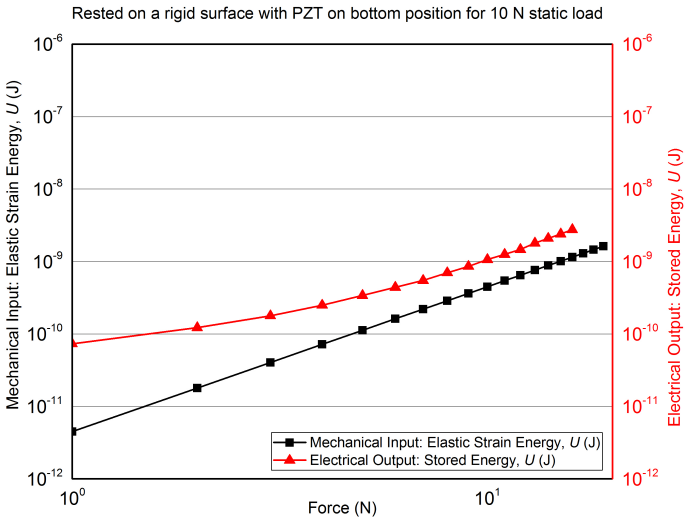

Figure 4.24: Comparison between the mechanical input and electrical output for the boundary condition-2 with the static load of 10 N

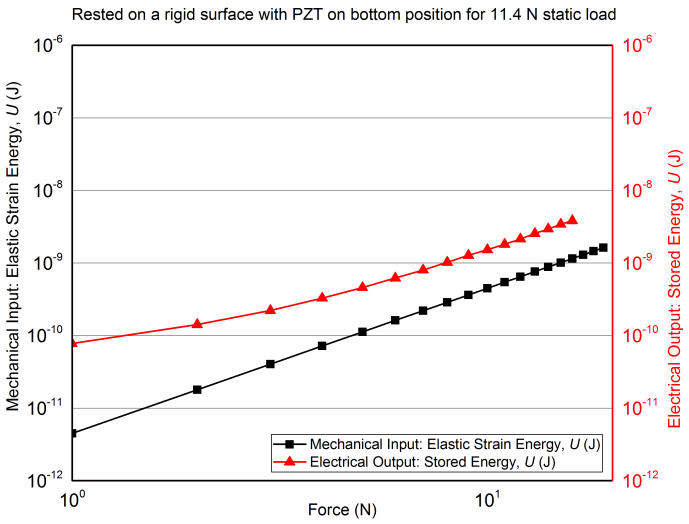

Figure 4.25: Comparison between the mechanical input and electrical output for the boundary condition-2 with the static load of 11.4 N

Figure 4.24 shows the comparison between the calculated mechanical input: elastic strain energy and the stored electrical output: stored energy for the boundary condition-2 with

the static load of 10 N. Nearly one order of magnitude difference is obtained between the calculated mechanical input and the stored electrical energy. During the stored electrical output measurement the piezoelectric buzzer is placed over the Berlincourt metal caliber, which is not a flat rigid surface could the reason for this discrepancy because it might slightly induce bending in the piezoelectric buzzer. Therefore this results in measuring high electrical output: stored energy. Further study is needed to fully understand this discrepancy. Similar pattern is obtained for the boundary condition-2 with the static load of 11.4 N and 13.4 N. The figure 4.25 and 4.26 shows the comparison for the boundary condition-2 for 11.4 N and 13.4 N static load.

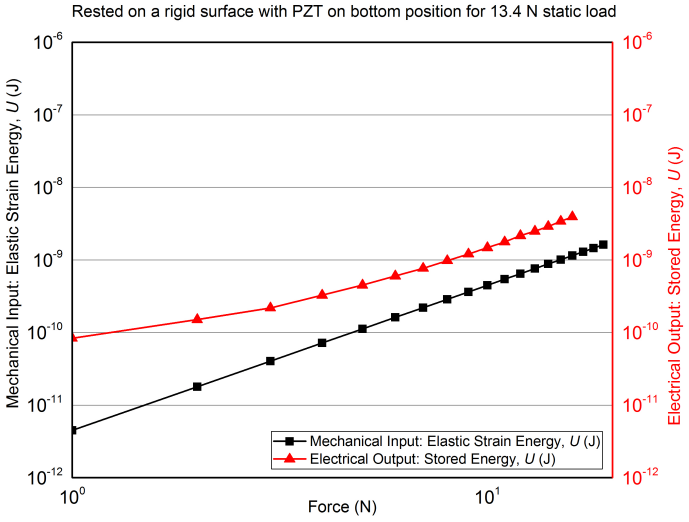

Figure 4.26: Comparison between the mechanical input and electrical output for the boundary condition-2 with the static load of 13.4 N

Chapter 5

Conclusion

The investigation on how the mechanical input energy varies for 4 different boundary conditions and how the boundary conditions influences the electrical output: stored energy, and the comparison of the calculated mechanical input energy and the stored electrical energy in 3 different static load have been studied. The main conclusions obtained are as follows:

Results for the mechanical input: elastic strain energy, U (J)

1. Analytically calculated mechanical input: elastic strain energy for the boundary condition-3 and 4, which involves bending effect in the piezoelectric structure, shows a significant increase of two order of magnitude higher elastic strain energy when compared to boundary condition-1 and 2.

2. The analytical approach used for the boundary condition 1 and 2 makes a good agreement with $1/2 \times d_{33} g_{33} (F/A)^2$ curve.

Results for the electrical output: stored energy, U (J)

3. The experimentally measured electrical output: stored energy for the boundary condition 3, which involves bending, shows a significant increase of three order of magnitude higher electrical output when compared to boundary condition-1 and 2.

4. The non-linearity for the electrical output in the boundary condition-4 is due to the fracture in the PZT layer on the very first application of the load. The fracture is caused by subjecting the PZT layer in the tensile loading condition. The capacitance measurement and the load vs displacement experiment confirms the fracture in the PZT structure.

5. The bending due to the ring support in the boundary condition-3 yields one order of magnitude lesser stored electrical output when compared to the stored electrical output obtained for the unimorph cantilever configuration found by Deutz [17].

Results for the comparison of mechanical input strain energy and stored electrical output energy in all boundary conditions

6. The measured stored electrical energy is higher than the analytically calculated mechanical input: elastic strain energy for the boundary condition 1 and 2. This is due to slight involvement of bending in the piezoelectric structure during the stored electrical energy measurement. Further study on this is required.

7. Less disparity in the comparison for the boundary condition-3 is seen for all the values of the applied load and the analytical method used for boundary condition-3 is more reliable.

8. In the case of boundary condition-4, the disparity between the mechanical input and the stored electrical output is due to the fracture of PZT at the very first application of the load. The analytical method used for the boundary condition-4 is also more reliable.

The maximum load bearing capacity for all boundary conditions

9. No fracture is observed in the boundary condition-1 and 2 for the load applied up to 1 kN. It is determined by the uniaxial compression test. Absence of bending involves no fracture in the PZT layer.

10. The maximum load bearing capacity for the PZT layer in the boundary condition-3 is 180 N. The PZT layer is subjected to compressive loading in boundary condition-3.

11. The maximum load bearing capacity for the PZT layer in the boundary condition-4 is 10 N. Subjecting the PZT layer in the tensile loading condition reduces the maximum load bearing capacity.

Recommendations for future work

1. To predict the mechanical input: elastic strain energy more accurately, FEA analysis for elastic strain energy prediction can be incorporated in future.

2. Slight bending involved during the measurement of electrical output: stored energy for the boundary condition-1 and 2 can be avoided by making the resting surface flat.

3. The above mentioned work can be extended in the direction of changing the inactive layer of the buzzer to enhance the bending in the structure for increasing the electrical output: stored energy.

Appendix A

Appendix

A.1 The effect of increasing the pre-static load on the electrical output for the boundary condition-1,2,3

As we have discussed before in the chapter-3, the effect of increasing the DC offset voltage would increases the pre-static load applied along with the quasi static load. The DC offset voltage is converted in terms of pre-static load by the relation

$$\text{Static Load (N)} = 2 \times V_{DC} + 1.4\text{N} \tag{A.1}$$

Increasing the pre-static load from the DC offset voltage applied along with the varying quasi static load increases the electrical output: stored energy experienced by the PZT layer. Thus increasing electrical output trend for the increased pre static load is seen for all the boundary conditions used and it is shown in the figure A.1, A.2, A.3.

A.1.1 The effect of increasing the static load on the stored electrical energy for the boundary condition-1,2 and 3

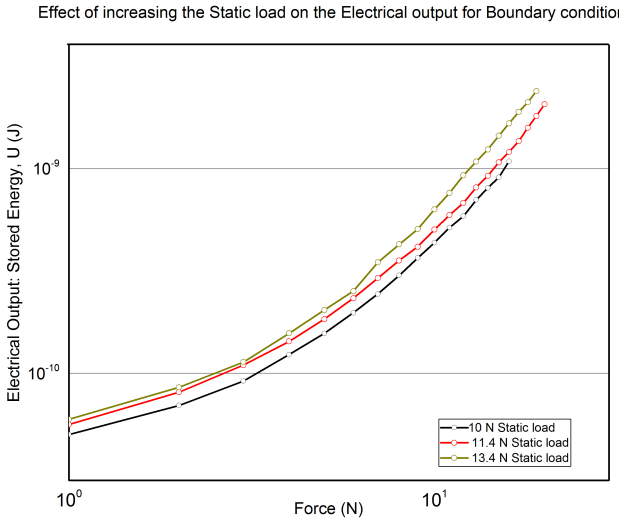

Figure A.1: Effect of increasing the static load on the stored electrical output for Boundary condition-1

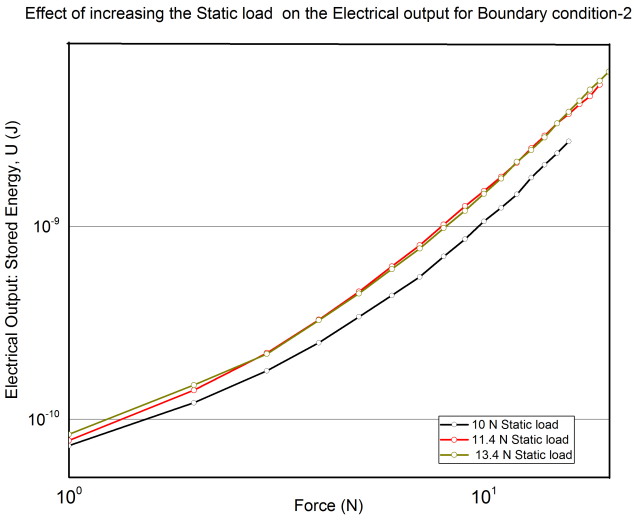

Figure A.2: Effect of increasing the static load on the stored electrical output for Boundary condition-2

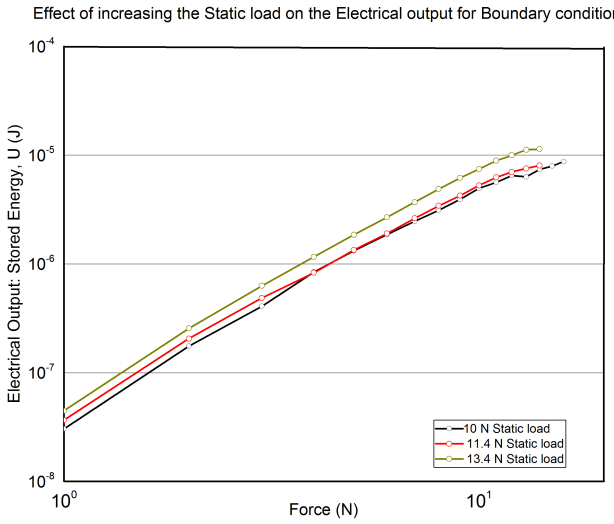

Figure A.3: Effect of increasing the static load on the stored electrical output for Boundary condition-3

A.2 Finite Element analysis for determining the stress distribution

Finite element analysis using Abaqus is carried out for determining the average biaxial stress distribution trend along the radial distance for the PZT layer in boundary condition-3 subjected to bending. The main reason for carrying out this FEA analysis stress distribution is to compare with the trend obtained analytically for the boundary condition-3. Load of 20 N is applied on the piezobuzzer for the boundary condition-3. The average biaxial stress in the PZT layer has the maximum value at the centre and it decays with the distance from the center and it is shown in the figure A.4.

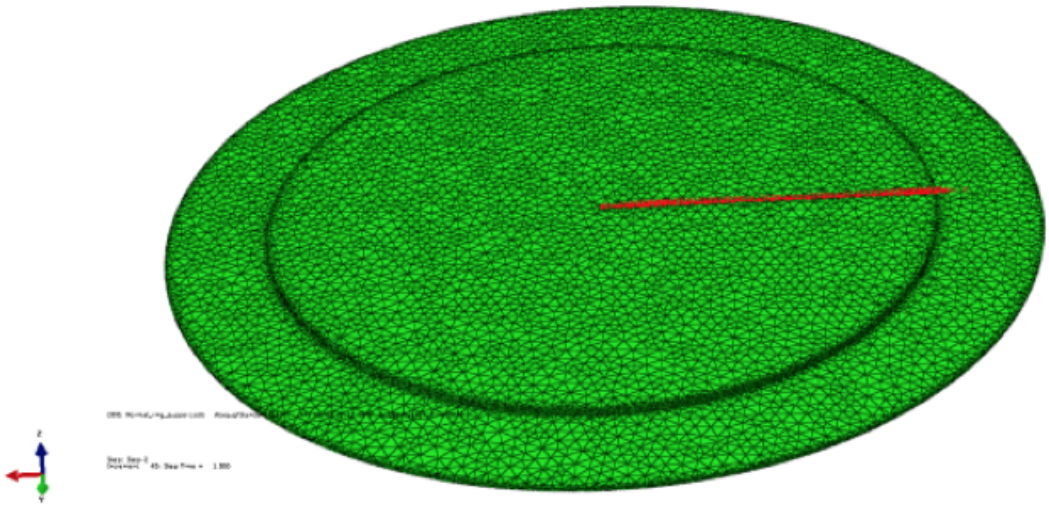

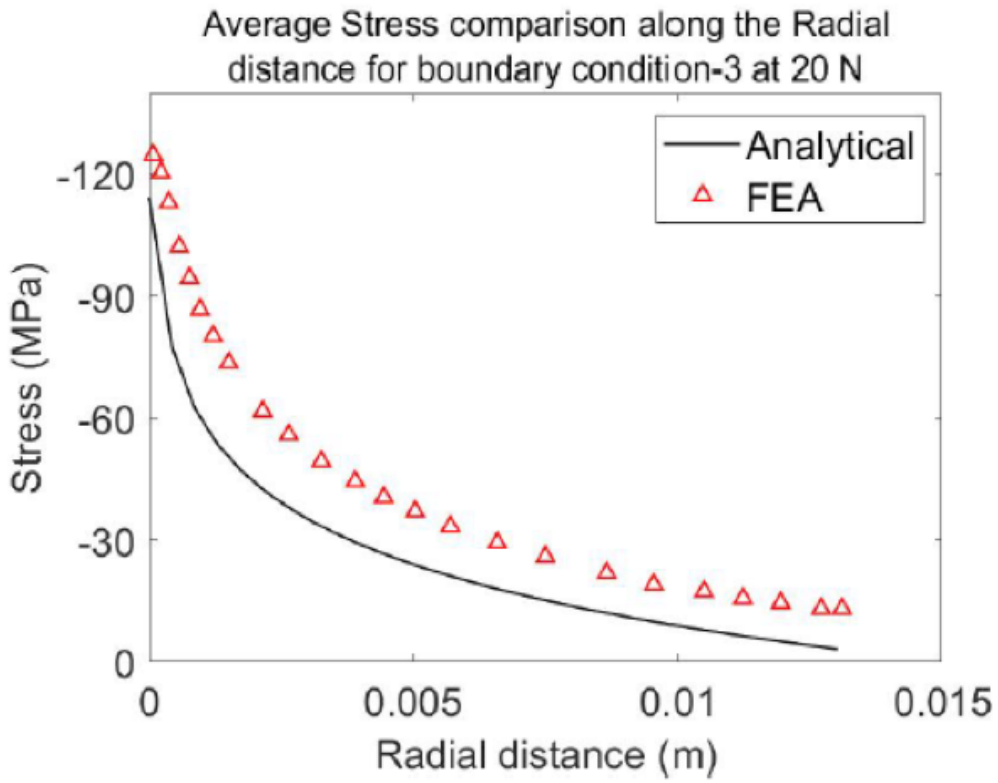

Figure A.4: Average stress distribution comparison in the PZT layer for the boundary condition-3 obtained using FEA analysis and analytical model at 20 N

The average stress distribution along the radial distance obtained from the analytical model for the boundary condition-3 is slightly lower than the average stress distribution found using the FEA analysis. The trend predicted with the FEA analysis and analytical model is same along the radial distance. So, the analytical model used for the boundary condition 3 and 4 are more reliable.

A.3 Biaxial stress distribution using analytical solution along the radial distance of the PZT layer in boundary condition- 3 and 4

A.3.1 Biaxial stress distribution in boundary condition-3 and 4 at 1 N

The analytically calculated thickness averaged hoop stress($\overline{\sigma}_\theta$) and radial stress($\overline{\sigma}_r$)along the radial distance of the PZT layer for the boundary condition-3 at 1N is shown in the figure A.5. The PZT layer is subjected to compressive load and the maximum hoop stress($\overline{\sigma}_\theta$) and radial stress($\overline{\sigma}_r$) reached is -7 MPa and these stresses decays along the radial distance and reaches 0 for $\overline{\sigma}_r$ at r=0.013m.

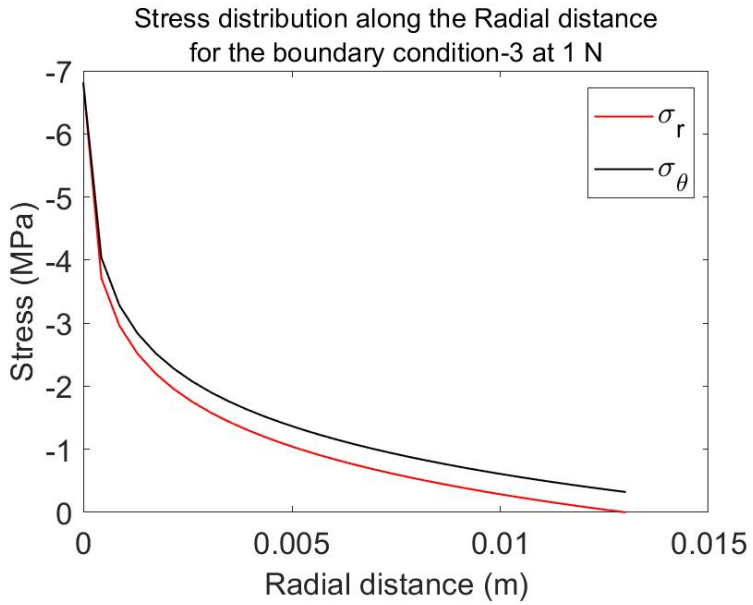

Figure A.5: Analytically calculated stress distribution for 1 N along the radial length in the PZT layer for the boundary condition-3

The analytically calculated thickness averaged hoop and radial stress along the radial distance for the boundary condition-4 at 1 N is shown in the figure A.6. Here in this

case, the PZT layer is in tensile condition and the maximum hoop stress($\overline{\sigma}_\theta$) and radial stress($\overline{\sigma}_r$) reached is 12 MPa at the hertzian contact area and these stresses decays along the radial distance and reaches 0 for $\overline{\sigma}_r$ at r=0.013m.

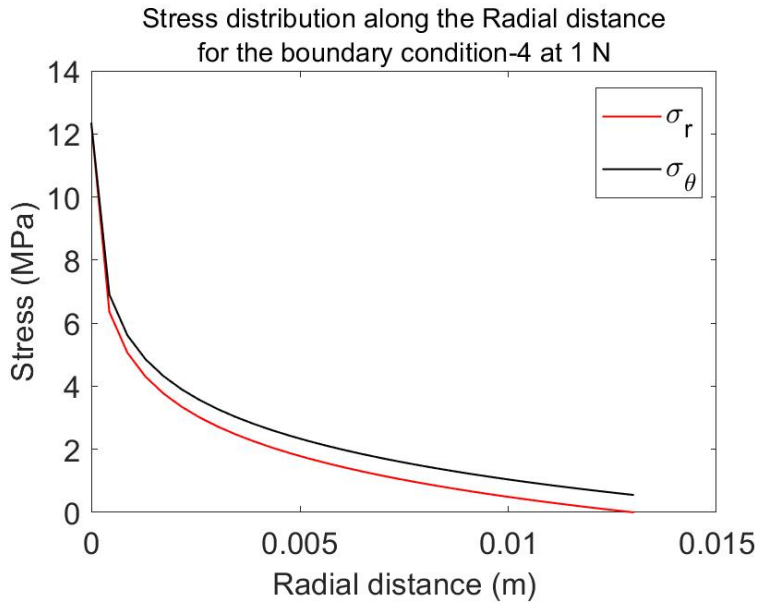

Figure A.6: Analytically calculated stress distribution for 1 N along the radial length in the PZT layer for the boundary condition-4

A.3.2 Analytically calculated stress distribution along the radial length in the PZT layer at the critical load for the boundary condition-3 and 4

The analytically calculated hoop stress($\overline{\sigma}_\theta$) and radial stress($\overline{\sigma}_r$)along the radial distance of the PZT layer for the boundary condition-3 at 180 N is shown in the figure A.7. The maximum load bearing capacity of the PZT layer in the boundary condition-3 is determined as 180N from the ball-on-the ring mechanical test. The analytically calculated maximum hoop stress($\overline{\sigma}_\theta$) and radial stress($\overline{\sigma}_r$) for the PZT layer at 180 N is -820 MPa, which has reached a value higher than -570 MPa as mentioned in the literature [20]. This results in the fracture of the PZT layer.

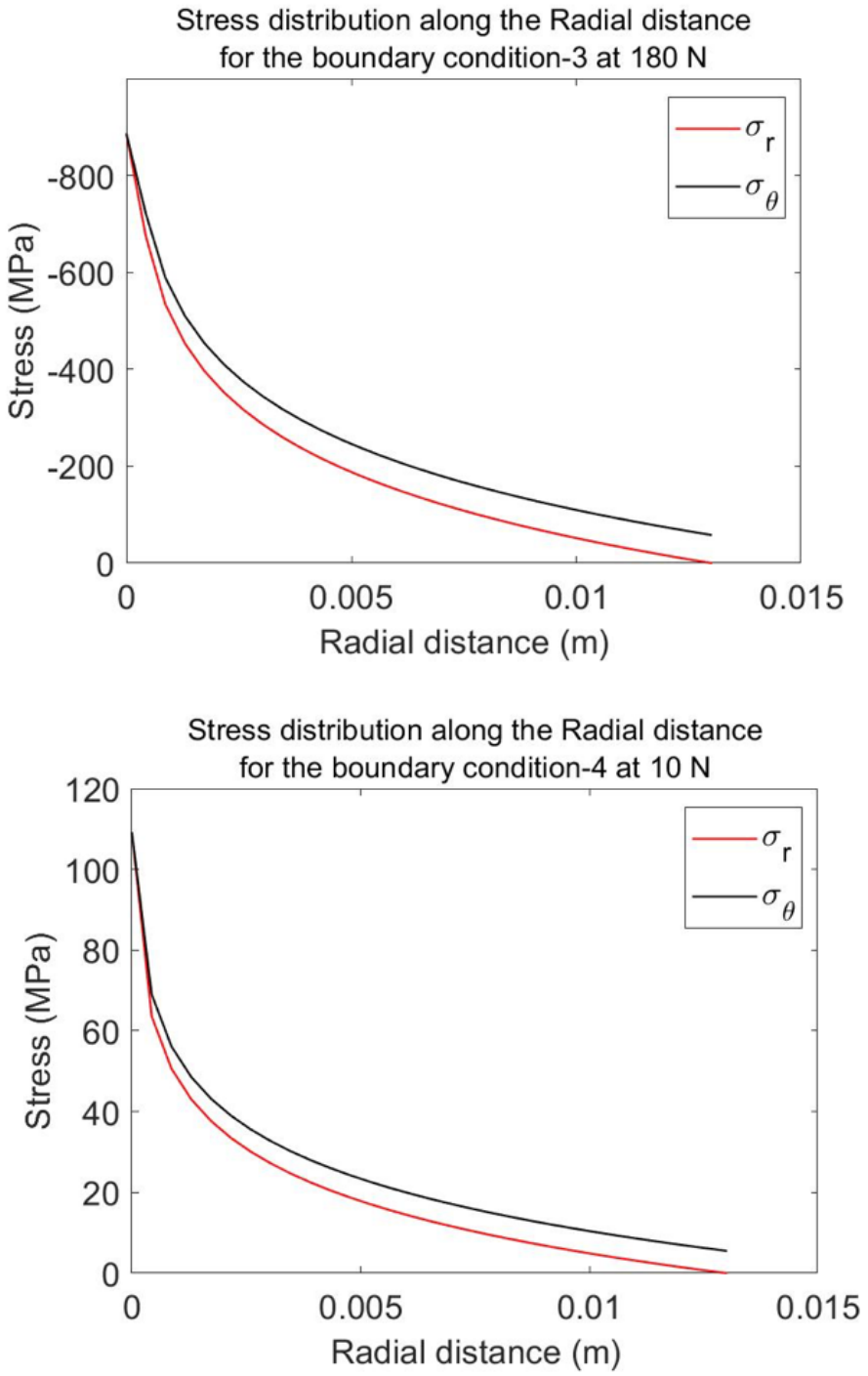

Figure A.7: Analytically calculated stress distribution for the boundary condition-3 and 4 at its critical mechanical load

The analytically calculated hoop stress($\overline{\sigma}_\theta$) and radial stress($\overline{\sigma}_r$)along the radial distance of the PZT layer for the boundary condition-4 at 10 N is shown in the figure A.7. The maximum load bearing capacity of the PZT layer in the boundary condition-4 is determined as 10 N from the ball-on-the ring mechanical test. The analytically calculated maximum hoop stress($\overline{\sigma}_\theta$) and radial stress($\overline{\sigma}_r$) for the PZT layer at 10 N is 110 MPa, which has reached higher tensile strength than 74.8 MPa as mentioned in the literature [20]. This results in the fracture of the PZT layer.

Bibliography

[1] A. Veronica, "These new materials are powering the battery revolution," https://www.weforum.org/agenda/2018/10/new-materials-are-powering-the-battery-revolution/, 2018-10-29.

[2] E. Jonathan, "Batteries can be the fight against climate change," www.weforum.org/agenda/2017/11/battery-batteries-electric-cars-carbon-sustainable-power-energy/, 28-10-2018.

[3] M. Ferrari, V. Ferrari, M. Guizzetti, and D. Marioli, "An autonomous battery-less sensor module powered by piezoelectric energy harvesting with rf transmission of multiple measurement signals," *Smart Materials and Structures*, vol. 18, no. 8, p. 085023, 2009.

[4] G. Park, T. Rosing, M. D. Todd, C. R. Farrar, and W. Hodgkiss, "Energy harvesting for structural health monitoring sensor networks," *Journal of Infrastructure Systems*, vol. 14, no. 1, pp. 64–79, 2008.

[5] M. Renaud, P. Fiorini, R. van Schaijk, and C. Van Hoof, "Harvesting energy from the motion of human limbs: the design and analysis of an impact-based piezoelectric generator," *Smart Materials and Structures*, vol. 18, no. 3, p. 035001, 2009.

[6] N. S. Shenck and J. A. Paradiso, "Energy scavenging with shoe-mounted piezoelectrics," *IEEE micro*, vol. 21, no. 3, pp. 30–42, 2001.

[7] S. Roundy, P. K. Wright, and J. Rabaey, "A study of low level vibrations as a power source for wireless sensor nodes," *Computer Communications*, vol. 26, no. 11, pp. 1131–1144, 2003.

[8] S. Thiruvelselvan, "Energy Harvesting From A Piezoelectric Source To Power A Wireless System Senthil Kumar Thiruvelselvam," *MSc thesis, TU Delft*, 2018.

[9] S. P. Beeby, M. J. Tudor, and N. M. White, "Energy harvesting vibration sources for microsystems applications," *Measurement Science and Technology*, vol. 17, no. 12, 2006.

[10] C. R. Bowen, H. A. Kim, P. M. Weaver, and S. Dunn, "Piezoelectric and ferroelectric materials and structures for energy harvesting applications," *Energy and Environmental Science*, vol. 7, no. 1, pp. 25–44, 2014.

[11] H. Li, C. Tian, and Z. D. Deng, "Energy harvesting from low frequency applications using piezoelectric materials," *Applied Physics Reviews*, vol. 1, no. 4, 2014.

[12] S. Priya, "Advances in energy harvesting using low profile piezoelectric transducers," *Journal of Electroceramics*, vol. 19, no. 1, pp. 165–182, 2007.

[13] T. Rodig, A. Schonecker, and G. Gerlach, "A survey on piezoelectric ceramics for generator applications," *Journal of the American Ceramic Society*, 2010.

[14] S. Roundy, P. K. Wright, and J. Rabaey, "A study of low level vibrations as a power source for wireless sensor nodes," *Computer Communications*, vol. 26, no. 11, pp. 1131–1144, 2003.

[15] H. A. Sodano, D. J. Inman, and G. Park, "A review of power harvesting from vibration using piezoelectric materials," *Shock and Vibration Digest*, vol. 36, no. 3, pp. 197–205, 2004.

[16] K. Uchino, "Piezoelectric energy harvesting systems—essentials to successful developments," *Energy Technology*, vol. 6, no. 5, pp. 829–848, 2018.

[17] D. B. Deutz, J.-A. Pascoe, B. Schelen, S. van der Zwaag, D. M. de Leeuw, and P. Groen, "Analysis and experimental validation of the figure of merit for piezoelectric energy harvesters," *Materials Horizons*, vol. 5, no. 3, pp. 444–453, 2018.

[18] K. Uchino, "Glory of piezoelectric perovskites," *Science and Technology of Advanced Materials*, vol. 16, no. 4, p. 046001, 2015.

[19] J. Rödel, K. G. Webber, R. Dittmer, W. Jo, M. Kimura, and D. Damjanovic, "Transferring lead-free piezoelectric ceramics into application," *Journal of the European Ceramic Society*, vol. 35, no. 6, pp. 1659–1681, 2015.

[20] D. Munz and T. Fett, *Ceramics: mechanical properties, failure behaviour, materials selection*. Springer Science & Business Media, 2013, vol. 36.

[21] J. Holterman and P. Groen, *An Introduction to piezoelectric materials and Applications*. Stichting Applied Piezo, the Netherlands, ISBN: 978-90-819361-1-8, 2013.

[22] A. Shaji Karapuzha, "Exploration of Non-MPB PZT compositions for high piezoelectric voltage sensitive 0-3 composites," *MSc thesis, TU Delft*, 2014.

[23] F. Van Loock, "Exploring the opportunities of piezoelectric composites for shear strain-driven energy harvesting," *MSc thesis, TU Delft*, 2014.

[24] B. Jafffe, W. R. Cook Jr, and H. Jaffe, *Piezoelectric Ceramics*, 2012, vol. 3: Elsevier.

[25] A. Meitzler, D. Berlincourt, F. Welsh, H. Tiersten, G. Coquin, and A. Warner, "IEEE Standard on Piezoelectricity: An American National Standard. Std 176, 66 p," *IEEE-ANSI, New York, USA*, 1987.

[26] A. Vázquez Carazo, "Novel piezoelectric transducers for high voltage measurements," *Doctral thesis, Universitat Politècnica de Catalunya*, 2000.

[27] J. Peter, "Fundamentals of piezo stack actuator," https://www.piezotechnics.com/piezo-technology/piezo-stack-actuator/, 28-10-2018.

[28] A. Safari, B. Jadidian, and E. Akdogan, "Piezoelectric composites for transducer applications," *Elsevier*, 2000.

[29] H. W. Kim, A. Batra, S. Priya, K. Uchino, D. Markley, R. E. Newnham, and H. F. Hofmann, "Energy harvesting using a piezoelectric "cymbal" transducer in dynamic environment," *Japanese Journal of Applied Physics*, vol. 43, no. 9R, p. 6178, 2004.

[30] J. Cho, R. Richards, D. Bahr, C. Richards, and M. Anderson, "Efficiency of energy conversion by piezoelectrics," *Applied Physics Letters*, vol. 89, no. 10, p. 104107, 2006.

[31] J. Ajitsaria, S.-Y. Choe, D. Shen, and D. Kim, "Modeling and analysis of a bimorph piezoelectric cantilever beam for voltage generation," *Smart Materials and Structures*, vol. 16, no. 2, p. 447, 2007.

[32] A. Erturk and D. J. Inman, "An experimentally validated bimorph cantilever model for piezoelectric energy harvesting from base excitations," *Smart Materials and Structures*, vol. 18, no. 2, p. 025009, 2009.

[33] C. Mo, J. Davidson, and W. W. Clark, "Energy harvesting with piezoelectric circular membrane under pressure loading," *Smart Materials and Structures*, vol. 23, no. 4, p. 045005, 2014.

[34] P. Cornwell, J. Goethal, J. Kowko, and M. Damianakis, "Enhancing power harvesting using a tuned auxiliary structure," *Journal of Intelligent Material Systems and Structures*, vol. 16, no. 10, pp. 825–834, 2005.

[35] C. Hsueh, M. Lance, and M. Ferber, "Stress distributions in thin bilayer discs subjected to ball-on-ring tests," *Journal of the American Ceramic Society*, vol. 88, no. 6, pp. 1687–1690, 2005.

[36] "Standard test method for monotonic equibiaxial flexural strength of advanced ceramics at ambient temperature," ASTM 1499-03.

[37] W. S. Geertsma, "Mechanical Aspects of Wafer-Based Crystalline Silicon Solar Cells," *MSc thesis, TU Delft*, 2013.

[38] "Standard test method for monotonic compressive strength of advanced ceramics at ambient temperature," ASTM C1424.

[39] B. Daniel, "Physical and piezoelectric properties of apc materials," https://www.americanpiezo.com/apc-materials/piezoelectric-properties.html, 28-10-2018.

[40] D. Fabris, J. C. Souza, F. S. Silva, M. Fredel, J. Mesquita-Guimarães, Y. Zhang, and B. Henriques, "The bending stress distribution in bilayered and graded zirconia-based dental ceramics," *Ceramics International*, vol. 42, no. 9, pp. 11 025–11 031, 2016.

[41] S. P. Timoshenko and S. Woinowsky-Krieger, *Theory of plates and shells*. McGraw-hill, 1959.

[42] C.-H. Hsueh, C. R. Luttrell, and P. F. Becher, "Analyses of multilayered dental ceramics subjected to biaxial flexure tests," *Dental Materials*, vol. 22, no. 5, pp. 460–469, 2006.

[43] "Young's modulus - tensile and yield strength for common materials," https://www.engineeringtoolbox.com, 28-10-2018.

[44] R. G. Budynas, J. K. Nisbett *et al.*, *Shigley's mechanical engineering design*. McGraw-Hill New York, 2008, vol. 8.

[45] H. Fessler and D. Fricker, "A theoretical analysis of the ring-on-ring loading disk test," *Journal of the American Ceramic Society*, vol. 67, no. 9, pp. 582–588, 1984.

[46] P. Kelly, "Solid mechanics lecture notes - *University of Auckland*," http://homepages.engineering.auckland.ac.nz/~pkel015/SolidMechanicsBooks/Part_II/04_ElasticityPolar/ElasticityPolars_Complete.pdf, 28-10-2018.